Shell Model Approaches: From $N = Z$ Towards the Neutron Drip Line

1

Alfredo Poves and Frédéric Nowacki

Abstract

The shell model with large-scale configuration mixing (SM-CI) is the theoretical tool of choice in nuclear spectroscopy. In this chapter, we introduce its basic concepts and discuss our present understanding of the model in terms of the competition between the spherical mean field and the nuclear correlations. A key aspect we shall treat is the choice of the valence spaces and effective interactions. We shall discuss as well the main collective modes of the nucleus—superfluidity, associated with the pairing interaction and vibrations and rotations originating in the multipole-multipole terms—using simple models. The emergence of permanent quadrupole deformation and rotational bands brings us to study Elliott's model and some of its variants. These models make it possible to give a physically intuitive interpretation of the full-fledged SM-CI calculations. First, we examine the cases of shape coexistence in two paradigms of doubly magic nuclei, ^{40}Ca and ^{56}Ni. We then move into the neutron-rich regime, to study the mechanisms that lead to the appearance of islands of inversion (IoI) at $N = 40$ and $N = 50$ and its relationship with the phenomenon of shape coexistence in ^{68}Ni and ^{78}Ni.

A. Poves (✉)
Departamento de Física Teórica and IFT UAM-CSIC, Universidad Autónoma de Madrid, Madrid, Spain
e-mail: alfredo.poves@uam.es

F. Nowacki
Université de Strasbourg, CNRS, IPHC UMR 7178, Strasbourg, France
e-mail: frederic.nowacki@iphc.cnrs.fr

S. M. Lenzi, D. Cortina-Gil (eds.), *The Euroschool on Exotic Beams, Vol. VI*,
Lecture Notes in Physics 1005, https://doi.org/10.1007/978-3-031-10751-1_1

1.1 Basic Concepts

In the standard model of nuclear structure, the elementary components are nucleons (N neutrons and Z protons, N+Z = A). The mesonic and quark degrees of freedom are integrated out. In most cases non-relativistic kinematics is used. The bare nucleon-nucleon (or nucleon-nucleon-nucleon) interactions are inspired by meson exchange theories or more recently by chiral effective field theory (χ-EFT) and must reproduce the nucleon-nucleon phase shifts and the properties of the deuteron and other few-body systems. The challenge is to find $\Psi(\mathbf{r}_1, \mathbf{r}_2, \mathbf{r}_3, \ldots \mathbf{r}_A)$ such that $H\Psi = E\Psi$, with

$$H = \sum_{i}^{A} T_i + \sum_{i,j}^{A} V_{2b}(\mathbf{r}_i, \mathbf{r}_j) + \sum_{i,j,k}^{A} V_{3b}(\mathbf{r}_i, \mathbf{r}_j, \mathbf{r}_k) \tag{1.1}$$

The knowledge of the eigenvectors Ψ and the eigenvalues E makes it possible to obtain electromagnetic moments, transition rates, weak decays, cross sections, spectroscopic factors, etc. The task is indeed formidable. Only recently and only for very light nuclei $A \leq 10$ the problem has been solved "exactly" thanks to the pioneer work of Pandharipande, Wiringa and Pieper [1], who used variational methods (Green function) solved by Monte Carlo (GFMC) techniques. The perturbative approach has been implemented in the framework of the no-core shell model (NCSM) by Barrett, Navratil and Vary [2]. And even more recently, the techniques of lattice gauge theory together with χ-EFT interactions have been used with very promising results in very light nuclei [3]. A mixed approach between the "ab initio" program based upon effective interactions obtained by χ-EFT, and the shell model with (large-scale) configuration mixing (SM-CI), is the valence-space in-medium similarity renormalization group (VS-IMSRG9 approach [4].

A very important outcome of these calculations is the compulsory need to include three-body forces in order to get correct solutions of the nuclear many-body problem. The GFMC and the NCSM approaches are severely limited by the huge size of the calculations when A becomes larger than 12. For the rest of the chart of nuclides, approximate methods have to be used. Except for the semi-classical ones (liquid drop) and the α-cluster models, all are based on the independent particle model (IPM). Beyond the limits of applicability of the fully "ab initio" descriptions, the methods of choice are the SM-CI and the beyond mean field (BFM) approaches using energy density functionals (a.k.a. density-dependent effective interactions, like the Gogny force). There are nowadays renewed efforts to connect rigorously these two global methods and the bare two- and three-body nuclear interactions by means of the full palette of the many-body perturbation methods. If this is achieved, they will deserve the "ab initio" label as well.

1.1.1 The Independent Particle Model

The basic idea of the independent particle model is to assume that, at the zeroth order, the result of the complicated two-body interactions among the nucleons is to produce an average self-binding potential. Mayer and Jensen (1949) proposed a spherical mean field consisting in the isotropic harmonic oscillator plus a strongly attractive spin-orbit potential and an orbit-orbit term:

$$H = \sum_i h(\mathbf{r}_i) \tag{1.2}$$

$$h(r) = -V_0 + \mathcal{T} + \frac{1}{2} m\omega^2 r^2 - V_{so}\mathbf{l}\cdot\mathbf{s} - V_B\mathbf{l}^2 \tag{1.3}$$

where we have used $\mathcal{T}$ for the kinetic energy to avoid confusion with the isospin quantum number T.

Later, other functional forms which follow better the form of the nuclear density and have a more realistic asymptotic behaviour, e.g. the Woods-Saxon (WS) well, were adopted:

$$V(r) = V_0 \left(1 + e^{\frac{r-R}{a}}\right)^{-1} \tag{1.4}$$

with

$$V_0 = \left(-51 + 33\frac{N-Z}{A}\right) \text{MeV} \tag{1.5}$$

and

$$V_{ls}(r) = \frac{V_0^{ls}}{V_0}(\mathbf{l}\cdot\mathbf{s})\frac{r_0^2}{r}\frac{dV(r)}{dr} \; ; \; V_0^{ls} = -0.44V_0 \tag{1.6}$$

The eigenvectors of the IPM are characterized by the radial quantum number n, the orbital angular momentum l, the total angular momentum j and its z projection m. With the choice of the harmonic oscillator, the eigenvalues are

$$\epsilon_{nljm} = -V_0 + \hbar\omega(2n + l + 3/2)$$

$$- V_{so}\frac{\hbar^2}{2}(j(j+1) - l(l+1) - 3/4) - V_B\hbar^2 l(l+1) \tag{1.7}$$

In order to reproduce the nuclear radii,

$$\hbar\omega = 45A^{-1/3} - 25A^{-2/3} \tag{1.8}$$

With a suitable choice of the parameters, it explains the magic numbers and, in the large A limit, the volume, the surface and (half) the symmetry terms of the semi-empirical mass formula as well (more on that later).

The wave functions of the isotropic HO can be written as

$$\Psi_{nlm}(r,\theta,\phi) = \frac{1}{r}\, R_{nl}(r)\; Y_{lm}(\theta,\phi) \tag{1.9}$$

By convention the ns start at zero; therefore the eigen-energies read:

$$E_{nl} = (2n + l + 3/2)\;\hbar\omega = (p + 3/2)\hbar\omega \tag{1.10}$$

$Y_{lm}(\theta,\phi)$ are the spherical harmonics and

$$R_{nl}(r) = (-1)^l \left(\frac{2\;(2\nu)^{l+3/2}\;n!}{\Gamma(n+l+3/2)}\right)^{1/2} r^{l+1}\; e^{-\nu r^2}\; L_n^{l+1/2}(2\nu r^2) \tag{1.11}$$

The parameter ν is defined as $\dfrac{m\omega}{2\hbar}$, and it is related to the length parameter of the HO $2\nu = \dfrac{1}{b^2}$. The degeneracy of each shell is $(p+1)(p+2)$, and the functions L are the Laguerre (associated) polynomials.

When the spin-orbit coupling is taken into account, we must include explicitly the spin part of the wave function and change the coupling scheme from [**L S**] to [**J J**]:

- VOCABULARY
  - STATE: a solution of the Schrödinger equation with a one-body potential, e.g. HO or WS. It is characterized by the quantum numbers $nljm$ and by its neutron or proton nature (or equivalently by the projection of the isospin t_z).
  - ORBIT: the ensemble of states with the same nlj, e.g. the $0d_{5/2}$ orbit. Its degeneracy is $(2j+1)$.
  - SHELL: an ensemble of orbits quasi-degenerated in energy, e.g. the sd-shell, that includes the orbits $0d_{5/2}$, $1s_{1/2}$ and $0d_{3/2}$.
  - MAGIC NUMBERS: the numbers of protons or neutrons that fill orderly a certain number of shells. For instance, 28 corresponds to the filling of the $s(2)$, $p(6)$ and $sd(12)$ shells plus the orbit $0f_{7/2}(8)$ and 50 to the filling of the s, p, sd, and $pf(20)$ shells plus the orbit $0g_{9/2}(10)$.
  - GAP: the energy difference between two shells.
  - SPE, single-particle energies: the eigenvalues of the IPM Hamiltonian.
  - ESPE, effective single-particle energies: the eigenvalues of the monopole Hamiltonian to be introduced in Sect. 1.4.

1.1.2 The Independent Particle Model and the Liquid-Drop Mass Formula

The IPM explains the magic numbers, spins and parities of the ground states and some excited states of doubly magic nuclei plus or minus one nucleon, their magnetic moments, etc. With the addition of a schematic pairing term between like particles, it can go a bit further in semi-magic nuclei (Schmidt lines). What is less well known is that in the large A limit, the IPM can reproduce the volume, the surface and the symmetry terms of the semi-empirical mass formula as well.

Let's take the IPM with an HO potential and neglect the spin-orbit term. Then

$$H = \sum_i \mathcal{T}_i - V_0 + \frac{1}{2} m\omega^2 r_i^2 \tag{1.12}$$

The single-particle energies are $\epsilon_i = -V_0 + \hbar\omega(p_i + 3/2)$ and $< r_i^2 >= b^2(p_i + 3/2)$ with $b^2 = \dfrac{\hbar}{m\omega}$.

Assuming $N = Z$, to accommodate $\frac{A}{2}$ identical particles, we need to fill all the shells up to a maximum value of $p = p_F$. Experimentally, the radius of the nucleus is given by $< r^2 >= \frac{3}{5}R^2 = \frac{3}{5}(1.2A^{1/3})^2$ and in the IPM by

$$< r^2 >= \frac{2}{A}\sum_i^{A/2} < r_i^2 >= \frac{2}{A}\sum_{p=0}^{p_F} b^2(p + 3/2)(p + 1)(p + 2) \tag{1.13}$$

From

$$\frac{A}{2} = \sum^{p_F}(p + 1)(p + 2) \tag{1.14}$$

it obtains at leading order

$$\frac{A}{2} = \frac{1}{3}{p_F}^3 \tag{1.15}$$

Hence, $p_F = (\frac{3}{2}A)^{1/3}$. Inserting this value in Eq. (1.13) it is easy to find that at leading order in p_F, $b^2 = A^{1/3}$ and $\hbar\omega = 41 \cdot A^{-1/3}$. We can now compute the total binding energy as

$$B = \sum_{i=1}^{A}(-V_0 + \hbar\omega(p_i + 3/2)) \tag{1.16}$$

that gives at leading order:

$$\frac{B}{A} + V_0 = \hbar\omega \cdot \frac{p_F^4}{4} \cdot \frac{2}{A} = \hbar\omega \left(\frac{3A}{2}\right)^{4/3} \frac{1}{2A} = \hbar\omega A^{1/3} \frac{1}{2} \left(\frac{3}{2}\right)^{4/3} \tag{1.17}$$

Finally we have

$$\frac{B}{A} = -V_0 + 41 \times 0.86 \tag{1.18}$$

and we recover the volume term of the semi-empirical mass formula for $V_0 \sim 50$ MeV.

If we go to next to leading order, keeping the terms in p_F^3, we recover the surface term and with a coefficient that agrees with the empirically determined one. We can repeat the calculation at leading order but with $N \neq Z$ and obtain

$$B = -AV_0 + \frac{\hbar\omega}{4}((p_F^\nu)^4 + (p_F^\pi)^4) = -AV_0 + \frac{\hbar\omega}{4}((3N)^{4/3} + (3Z)^{4/3}) \tag{1.19}$$

Making a Taylor expansion around the minimum at $N = Z$ and using the previously determined values, we find an extra term of the form $(N - Z)^2/A$ with a coefficient which does not agree with the one resulting from the fit of the semi-empirical mass formula to the experimental binding energies ($a_{sym} = 23$ MeV). This reflects the fact that the nuclear two-body neutron-proton interaction is in average more attractive than the neutron-neutron and the proton-proton ones, and it is related as well to the experimental evidence of the near equality of the neutron and proton radii for $N \neq Z$. Therefore we should use different values of $\hbar\omega$ and V_0s for protons and neutrons in the derivation, which complicates a lot the calculation because both effects go in opposite directions.

1.2 The Meaning of the Independent Particle Model

The usual procedure to generate a mean field in a system of N interacting fermions, starting from their free interaction, is the Hartree–Fock (HF) approximation, extremely successful in atomic physics. Whatever the origin of the mean field, the eigenstates of the N-body problem are Slater determinants, i.e. antisymmetrized products of N single-particle wave functions. In the nucleus, there is a catch, because the very strong short-range repulsion and the tensor force make the HF approximation based upon the bare nucleon-nucleon force impracticable. However, at low energy, the nucleus does manifest itself as a system of independent particles in many cases, and when it does not, it is due to the medium-range correlations that produce strong configuration mixing and not to the short-range repulsion. Does the success of the shell model really "prove" that nucleons move independently in a fully occupied Fermi sea as assumed in HF approaches? In fact, the single-particle

Table 1.1 The parameters of the Brink and Boeker interaction

i	μ_i(fm)	v_i (MeV)	m_i
1	0.7	471.1	−0.43
2	1.4	−163.8	0.51

motion can persist at low energies in fermion systems due to the suppression of collisions by the Pauli exclusion principle (see Pandharipande et al. [5]). Brueckner theory takes advantage of the Pauli blocking to regularize the bare nucleon-nucleon interaction, in the form of density-dependent effective interactions of use in HF calculations or G-matrices for large-scale shell model calculations.

An example of regularized interaction is the one proposed by Brink and Boeker [6], whose central part is

$$V_c(|\mathbf{r}_1 - \mathbf{r}_2|) = \sum_{i=1}^{2}[1 - m_i(1 + P_\sigma P_\tau)]\, v_i\, e^{-|\mathbf{r}_1-\mathbf{r}_2|^2/\mu_i^2} \tag{1.20}$$

where μ are the widths of the Gaussians and P the spin and isospin projectors. The values of m are fitted to produce the attraction in the S=0, T=1 and S=1, T=0 channels and repulsion in the others, whereas the vs give the energy scale of the two Gaussians. For the spin-orbit term, they took a one-body approximation (Table 1.1):

$$V_{ls} = \frac{-12\ \text{MeV}}{\hbar^2\sqrt{A}}\ \mathbf{l}\cdot\mathbf{s} \tag{1.21}$$

To be more realistic, one should refine the channel dependence of the central terms, include a two-body spin-orbit interaction and more importantly add a term which depends on the density. After this re-vamping, the Brink and Boeker interaction becomes the Gogny interaction [7] extremely successful in numerous mean field applications (and beyond).

The wave function of the ground state of a nucleus in the IPM is the product of a Slater determinant for the Z protons that occupy the Z lowest states in the mean field and another Slater determinant for the N neutrons in the N lowest states of the mean field. In the second quantization, this state can be written as

$$|N\rangle \cdot |Z\rangle \tag{1.22}$$

with

$$|N\rangle = n_1^\dagger n_2^\dagger \ldots n_N^\dagger |0\rangle \tag{1.23}$$

$$|Z\rangle = z_1^\dagger z_2^\dagger \ldots z_Z^\dagger |0\rangle \tag{1.24}$$

In a system of noninteracting fermions, the occupied states have occupation number 1, and the empty ones occupation number 0. In reality there is a dilution of the strength leading to a nonzero value above the Fermi level. In spite of that, the nuclear quasi-particles resemble extraordinarily to the mean field solutions of the IPM. This was demonstrated by the beautiful electron scattering experiment of Cavedon et al. [8] in which they extracted the charge density difference between ^{206}Pb and ^{205}Tl that in the IPM limit is just the square of the $2s_{1/2}$ orbit wave function. The shape of the $2s_{1/2}$ orbit is very well given by a mean field calculation with the Gogny functional. To make the agreement quantitative, the calculated density had to be scaled down with the occupation number. This is a first example of the necessity of using effective transition operators consistent with the regularized interactions that provide the natural basis for the many-body description of nuclei. For a very pedagogical discussion of the basis of the IPM, see Ref. [5].

1.3 Beyond the Independent Particle Model

It is quite obvious that the IPM cannot encompass the extreme variety of manifestations of the nuclear dynamics. In fact, even in the most favourable cases, as at the doubly magic nuclei, its limitations are dramatically evident. Let's take ^{40}Ca as an example. In the IPM limit, we expect a 0^+ ground state (no problem) and a gap of about $\hbar\omega$ (9 MeV) before finding a bunch of quasi-degenerate levels of particle-hole type and negative parity. In fact, the first excited state lies at 3.5 MeV and is again a 0^+, which, upon experimental and theoretical scrutiny, turns out to be the band head of a rotational band of 4p-4h nature. Even more exotic is another 0^+ at 5.1 MeV, which is the band head of a superdeformed band of 8p-8h structure. Going beyond the mean field is compulsory because the nuclear dynamics is dominated in most cases by the correlations. We shall show in what follows how these coexisting structures can be reproduced by large-scale shell model calculations and interpreted using analytic models.

To go beyond the IPM, there are two main routes: In the mean field way, the correlations are taken into account by explicitly breaking the symmetries of the mean field HF wave functions and employ density-dependent interactions of different sorts: Skyrme, Gogny or relativistic mean field parametrizations. They are often referred to as "intrinsic" descriptions. Projections before (VAP) or after (PAV) variation are enforced to restore the conserved quantum numbers. Ideally, configuration mixing is also implemented through the generator coordinate method. The other route pertains to the SM-CI which can be seen as an approximation to the exact solution of the nuclear A-body problem using effective interactions in restricted spaces. The SM-CI wave functions respect the symmetries of the Hamiltonian, and these approaches are sometimes called "laboratory frame" descriptions.

Let's proceed through a kind of formal solution to the A-body problem. The single-particle states $(i, j, k, \ldots)$, which are the solutions of the IPM, provide as well a basis in the space of the occupation numbers (Fock space). The many-body wave functions are Slater determinants:

$$\Phi = a_{i_1}^{\dagger}, a_{i_2}^{\dagger}, a_{i_3}^{\dagger}, \ldots a_{i_A}^{\dagger}|0\rangle \tag{1.25}$$

We can distribute the A particles in all the possible ways in the available single-particle states. This provides a complete basis in the Fock space. The number of Slater determinants will be huge but not infinite because the theory is no longer valid beyond a certain energy cut-off. Therefore, the "exact" solution can be expressed as a linear combination of the basis states:

$$\Psi = \sum_{\alpha} c_{\alpha} \Phi_{\alpha} \tag{1.26}$$

and the solution of the many-body Schödinger equation

$$H\Psi = E\Psi \tag{1.27}$$

is transformed in the diagonalization of the matrix:

$$H_{\alpha,\beta} = \langle \Phi_{\alpha}|H|\Phi_{\beta}\rangle \tag{1.28}$$

whose eigenvalues and eigenvectors provide the "physical" energies and wave functions. A shell model calculation thus amounts to diagonalizing the effective nuclear Hamiltonian in the basis of all the Slater determinants that can be built distributing the valence particles in a set of orbits which is called "valence space". The orbits that are always full form the "core". If we could include all the orbits in the valence space (a full no-core calculation), we should get the "exact" solution. The effective interactions for SM-CI calculations are obtained from the bare nucleon-nucleon interaction by means of a regularization procedure aimed to soften the short-range repulsion. In other words, using effective interactions we can treat the A-nucleon system in a basis of independent quasi-particles. As we reduce the valence space, the interaction has to be renormalized again using many-body perturbation theory. Up to this point, these calculations can be labelled as "ab initio". In fact, the realistic NN interactions seem to be correct except for its simplest part, the monopole Hamiltonian responsible for the evolution of the spherical mean field. Therefore, we surmise that the three-body forces will mainly contribute to the monopole Hamiltonian.

The three basic ingredients of the SM-CI approach are then the effective interactions, the valence spaces and the algorithms and codes put at work to solve the huge computational challenges posed by the solution of this secular problem. See, for instance, Ref. [9] for a full-fledged presentation of our approach.

1.4 The Effective Interactions in Fock Space

Using the creation and annihilation operators of particles in the states of the underlying spherical mean field in the coupled representation, we can write the Hamiltonian as

$$\mathcal{H} = \sum_{rr'} \epsilon_{rr'} (a_r^+ a_{r'})^0 + \sum_{r \le s, t \le u, \Gamma} W^{\Gamma}_{rstu} Z^+_{rs\Gamma} \cdot Z_{tu\Gamma} \tag{1.29}$$

where Z^+_Γ (Z_Γ) is the coupled product of two creation (annihilation) operators:

$$Z^+_{rs\Gamma} = [a^\dagger_r a^\dagger_s]^\Gamma \tag{1.30}$$

Γ is a shorthand for (J,T), r, s ... run over the orbits of the valence space, $\epsilon_{rr'}$ are the single-particle energies (or the kinetic energies in the no-core calculations) and W^{Γ}_{rstu} the antisymmetrized two-body matrix elements:

$$W^{\Gamma}_{rstu} = \langle j_r j_s (JT) | V | j_t j_u (JT) \rangle \tag{1.31}$$

In the occupation number representation (Fock space), all the information about the interaction is contained in its two-body matrix elements. The many-body problem then reduces to the manipulation of the creation and annihilation operators using the Wick theorem and techniques alike.

The most general method to compute the two-body matrix elements is due to Slater and carries his name. When the independent particle wave functions are those of the harmonic oscillator or if they can be represented by linear combination of a few harmonic oscillator states, the method of choice is that of Brody and Moshinsky [10]. Both methods are described in detail in Ref. [11].

1.4.1 Monopole and Multipole Components of the Interaction

Without losing the simplicity of the Fock space representation, we can recast the two-body matrix elements of any effective interaction in a way full of physical insight, following Dufour–Zuker rules [12].

"Any effective interaction can be split in two parts:

$$\mathcal{H} = \mathcal{H}_m(monopole) + \mathcal{H}_M(multipole) \tag{1.32}$$

where $\mathcal{H}_m$ contains all the terms that are affected by a spherical Hartree–Fock variation; hence it is responsible for the global saturation properties and for the evolution of the spherical single-particle energies".

Considering two-body interactions only, we can write

$$\mathcal{H}_m = \sum \epsilon_i n_i + \sum \left[\frac{1}{(1+\delta_{ij})} a_{ij}\, n_i (n_j - \delta_{ij}) + \frac{1}{2} b_{ij} \left(T_i \cdot T_j - \frac{3n_i}{4} \delta_{ij} \right) \right] \tag{1.33}$$

where n_i and T_i are the number and isospin operators for the orbit i. The coefficients a and b are defined in terms of the centroïds (angular averages):

$$V_{ij}^T = \frac{\sum_J W_{ijij}^{JT}[J]}{\sum_J [J]} \tag{1.34}$$

as $a_{ij} = \frac{1}{4}(3V_{ij}^1 + V_{ij}^0)$, $b_{ij} = V_{ij}^1 - V_{ij}^0$, the sums running over Pauli allowed values $[J]$ is a shorthand for $(2j+1)$.

It is easy to verify that the expectation value of the full Hamiltonian in a Slater determinant for closed shells has the same expression than the Hartree–Fock energy:

$$\langle H \rangle = \sum_i \langle i|\mathcal{T}|i\rangle + \sum_{ij} \langle ij|V|ij\rangle \tag{1.35}$$

where i and j run over the occupied states. $\mathcal{T}$ is the kinetic energy and V the effective interaction. If the two-body matrix elements are written in coupled formalism and we denote the orbits by $\alpha,\ \beta, \ldots$, the expression reads

$$\langle H \rangle = \sum_\alpha (2j_\alpha + 1)\langle \alpha|\mathcal{T}|\alpha\rangle + \sum_{\alpha \le \beta} \sum_{J,T} (2J+1)(2T+1)\langle j_\alpha j_\beta (JT)|V|j_\alpha j_\beta (JT)\rangle \tag{1.36}$$

The monopole Hamiltonian governs the evolution of effective spherical single-particle energies (ESPE) with the number of particles in the valence space, schematically:

$$\epsilon_j(\{n_i\}) = \epsilon_j(\{n_i = 0\}) + \sum_i a_{ij} n_i \tag{1.37}$$

Notice that the ESPEs not only evolve along isotopic and isotonic chains inside the valence space (shell evolution) but can change for different configurations in the same nucleus (configuration dependent or Type II shell evolution). It is very important to realize that even small defects in the centroids can produce large changes in the relative position of the different configurations due to the appearance of quadratic terms involving the number of particles in the different orbits.

The multipole Hamiltonian $\mathcal{H}_M$ can be written in two representations, particle-particle and particle-hole:

$$\mathcal{H}_M = \sum_{r\le s,t\le u,\Gamma} W^{\Gamma}_{rstu} Z^{+}_{rs\Gamma} \cdot Z_{tu\Gamma} \tag{1.38}$$

$$\mathcal{H}_M = \sum_{rstu\Gamma} [\gamma]^{1/2} \frac{(1+\delta_{rs})^{1/2}(1+\delta_{tu})^{1/2}}{4} \omega^{\gamma}_{rtsu} (S^{\gamma}_{rt} S^{\gamma}_{su})^0 \tag{1.39}$$

where S^{γ} is the product of one creation and one annihilation operator coupled to γ (i.e. $\lambda\tau$):

$$S^{\gamma}_{rs} = [a^{\dagger}_r a_s]^{\gamma} \tag{1.40}$$

The W and ω matrix elements are related by a Racah transformation:

$$\omega^{\gamma}_{rtsu} = \sum_{\Gamma} (-)^{s+t-\gamma-\Gamma} \begin{Bmatrix} r & s & \Gamma \\ u & t & \gamma \end{Bmatrix} W^{\Gamma}_{rstu} [\Gamma] \tag{1.41}$$

$$W^{\Gamma}_{rstu} = \sum_{\gamma} (-)^{s+t-\gamma-\Gamma} \begin{Bmatrix} r & s & \Gamma \\ u & t & \gamma \end{Bmatrix} \omega^{\gamma}_{rtsu} [\gamma] \tag{1.42}$$

The operators $S^{\gamma=0}_{rr}$ are just the number operators for the orbits r and the terms $S^{\gamma=0}_{rr'}$ produce the spherical Hartree–Fock particle-hole jumps. The latter must have null coefficients if the monopole Hamiltonian satisfies the Hartree–Fock self-consistency. The operator $Z^{+}_{rr\Gamma=0}$ creates a pair of particle coupled to $J = 0$. The terms $W^{\Gamma}_{rrss}\ Z^{+}_{rr\Gamma=0} \cdot Z_{ss\Gamma=0}$ represent different kinds of pairing Hamiltonians. The operators S^{γ}_{rs} are typical one-body operators of multipolarity γ. For instance, $\gamma = (J = 1, L = 0, T = 1)$ contains a $(\boldsymbol{\sigma} \cdot \boldsymbol{\sigma})$ $(\boldsymbol{\tau} \cdot \boldsymbol{\tau})$ term which is nothing else but the Gamow-Teller component of the nuclear interaction. The terms $S^{\gamma}_{rs}\gamma = (J = 2, T = 0)$ are of quadrupole type $r^2 Y_2$. They are responsible for the existence of deformed nuclei, and they are specially large and attractive when $j_r - j_s = 2$ and $l_r - l_s = 2$.

A careful analysis of the available realistic effective nucleon-nucleon interactions obtained with different methods reveals that the multipole Hamiltonian is universal and dominated by BCS-like isovector and isoscalar pairing plus quadrupole-quadrupole and octupole-octupole terms of very simple nature $(r^{\lambda} Y_{\lambda} \cdot r^{\lambda} Y_{\lambda})$. As an example we list in Table 1.2 the strengths of the coherent multipole components of different interactions for the pf-shell.

Table 1.2 Strengths (in MeV) of the coherent multipole components of different interactions for the *pf*-shell

	Particle-particle		Particle-hole		
Interaction	$JT = 01$	$JT = 10$	$\lambda\tau = 20$	$\lambda\tau = 40$	$\lambda\tau = 11$
KB3	−4.75	−4.46	−2.79	−1.39	+2.46
FPD6	−5.06	−5.08	−3.11	−1.67	+3.17
GOGNY	−4.07	−5.74	−3.23	−1.77	+2.46
GXPF1	−4.18	−5.07	−2.92	−1.39	+2.47
BONNC	−4.20	−5.60	−3.33	−1.29	+2.70

1.4.2 Valence Spaces and Codes

An ideal valence space should incorporate the most relevant degrees of freedom for the nuclei under study and be computationally tractable. Classical $0\hbar\omega$ valence spaces are provided by the major oscillator shells *p*, *sd* and *pf*. As we move far from stability, other choices are compulsory; for instance, for the very neutron-rich nuclei around $N = 28$, a good choice is to take the *sd*-shell for protons and the *pf*-shell for neutrons, and for the very neutron-rich Cr, Fe, Ni and Zn, one should rather take $r_3 - (0g_{9/2}, 1d_{5/2})$ for the neutrons and *pf* for protons (in a major harmonic oscillator shell of principal quantum number *p*, the orbit $j = p + 1/2$ is called $intruder$, and the remaining ones are denoted by r_p; for instance, in the *pf*-shell, the intruder orbit is the $0f_{7/2}$, and r_3 includes the orbits $1p_{3/2}$, $1p_{1/2}$ and $0f_{5/2}$). To describe the intruders around *N* and/or $Z = 20$, a good valence space is $r_2 - pf$. For the nuclei above ^{100}Sn, the valence space $r_4 - h_{11/2}$ has been also widely used.

The solution of the secular problem of the SM-CI is computationally very demanding. Direct diagonalization is of very limited utility, and other algorithms like the Lanczos method, Monte Carlo shell model, quantum Monte Carlo diagonalization, density matrix renormalization group, etc., are employed. There are also a number of different extrapolation ansatzs. The Strasbourg-Madrid codes (Antoine, Nathan) [9] can deal with problems involving the basis of 10^{11} Slater determinants, using relatively modest computational resources. Other competitive codes which have been released publicly are Oxbash [13], Nushell [14] and Kshell [15].

1.5 Collectivity in Nuclei

For a given interaction, a many-body system would or would not display coherent features at low energy depending on the structure of the mean field around the Fermi level. So, when the spherical mean field around the Fermi surface favours the pairing interaction, as in the case of having only neutrons and protons on top

of a doubly magic core, the nucleus tends to become superfluid. However, if the quadrupole-quadrupole interaction is dominant, for instance, if both protons and neutrons are available in open orbits, the nucleus acquires permanent deformation. In the extreme (unrealistic) limit in which the monopole Hamiltonian is negligible, the multipole interaction would maximize the deformation and together with the pairing interaction produce a kind of superfluid nuclear needles. Magic nuclei resist the strong multipole interaction, because the large gaps in the nuclear mean field at the Fermi surface block the correlations.

Let's consider a simple model consisting of two states that have diagonal energies that differ by Δ and an off-diagonal matrix element δ. The eigenvalues and eigenvectors of this problem are obtained diagonalizing the matrix:

$$\begin{pmatrix} 0 & \delta \\ \delta & \Delta \end{pmatrix} \tag{1.43}$$

In the limit $\delta << \Delta$, we can use perturbation theory, and no special coherence is found. On the contrary in the degenerate case, $\Delta \rightarrow 0$, the eigenvalues of the problem are $\pm\delta$, and the eigenstates are the 50% mixing of the unperturbed ones with different signs. They are the germ of the maximally correlated (or anticorrelated) states.

We can generalize this example by considering a degenerate case with N Slater determinants with equal (and attractive) diagonal matrix elements $(-\Delta)$ and off-diagonal ones of the same magnitude. The problem now is that of diagonalizing the matrix:

$$-\Delta \begin{pmatrix} 1 & 1 & 1 & \dots \\ 1 & 1 & 1 & \dots \\ 1 & 1 & 1 & \dots \\ . & . & . & \dots \\ . & . & . & \dots \\ . & . & . & \dots \end{pmatrix} \tag{1.44}$$

which has range 1 and whose eigenvalues are all zero except one which has the value $-N\Delta$. This is the coherent state. Its corresponding eigenvector is a mixing of the N unperturbed states with amplitudes $\frac{1}{\sqrt{N}}$.

1.5.1 Nuclear Superfluidity: Pairing Collectivity

The pairing Hamiltonian for one shell expressed in the m-scheme basis of two particles has a very similar matrix representation:

$$-G\begin{pmatrix} 1 & -1 & 1 & \dots \\ -1 & 1 & -1 & \dots \\ 1 & -1 & 1 & \dots \\ . & . & . & \dots \\ . & . & . & \dots \\ . & . & . & \dots \end{pmatrix} \tag{1.45}$$

and its coherent solution is just the state of the two particles coupled to zero which gains an energy $-G\Omega$ ($\Omega = j + 1/2$ is the degeneracy of the shell). It can be written as

$$Z_j^\dagger|0\rangle = \frac{1}{\sqrt{\Omega}}\sum_{m>0}(-1)^{j+m}a_{jm}^\dagger a_{j-m}^\dagger|0\rangle \tag{1.46}$$

Using the commutation relations,

$$\left[Z_j, Z_j^\dagger\right] = 1 - \frac{\hat{n}}{\Omega}; \quad \text{and} \quad \left[H, Z_j^\dagger\right] = -G(\Omega - \hat{n} + 2)Z_j^\dagger \tag{1.47}$$

where $\hat{n}$ is the operator number of particle, it is possible to construct the eigenstates of H for n particles consisting of $n/2$ pairs coupled to $J = 0$. These states are labelled as seniority zero states. The quantum number v (seniority) counts the number of particles not coupled to angular momentum zero:

$$|n, v = 0\rangle = (Z_j^\dagger)^{\frac{n}{2}}|0\rangle \quad \text{and} \quad E(n, v = 0) = -\frac{G}{4}n(2\Omega - n + 2) \tag{1.48}$$

We can construct also eigenstates with higher seniority using the operators $B_J^\dagger$ which create a pair of particles coupled to $J \neq 0$. These operators satisfy the relation:

$$\left[H, B_J^\dagger\right]|0\rangle = 0 \tag{1.49}$$

States which contain m $B_J^\dagger$ operators have seniority $v = 2m$. Their eigen-energies relative to the seniority zero state are

$$E(n, v) - E(n, v = 0) = \frac{G}{4}v(2\Omega - v + 2) \tag{1.50}$$

Notice that the gap is independent of the number of particles. The generalization to the odd number of particles is trivial.

For n protons and neutrons in the same shell of degeneracy Ω coupled to total isospin T, the eigenvalues of the $J = 0$ ($L = 0$) $T = 1$ pairing Hamiltonian can be written as

$$E(\Omega, n, v, t, T) = -G((n - v)(4\Omega + 6 - n - v)/8 + t(t + 1)/2 - T(T + 1)/2) \tag{1.51}$$

where v is the sum of the seniorities of protons and neutrons and t the reduced isospin, one half of their difference.

The case of two particles in several shells is also tractable and has a great heuristic value. The problem in a matrix form reads:

$$\begin{pmatrix} 2\epsilon_1 - G\Omega_1 & -G\sqrt{\Omega_1\Omega_2} & -G\sqrt{\Omega_1\Omega_3} \ldots \\ -G\sqrt{\Omega_2\Omega_1} & 2\epsilon_2 - G\Omega_2 & -G\sqrt{\Omega_2\Omega_3} \ldots \\ -G\sqrt{\Omega_3\Omega_1} & -G\sqrt{\Omega_3\Omega_2} & 2\epsilon_3 - G\Omega_3 \ldots \\ . & . & \ldots . \\ . & . & \ldots . \\ . & . & \ldots . \end{pmatrix} \tag{1.52}$$

There is a limit in which maximum coherence is achieved, when the orbits have the same Ω and they are degenerate. Then the coherent pair is evenly distributed among the shells, and its energy is $E = -G \sum_i \Omega$. All the other solutions remain at their unperturbed energies.

A textbook case of nuclear superfluidity is provided by the tin isotopes from $N = 52$ to $N = 80$. The five orbits comprised between the magic closures 50 and 82 are closely packed, and one should expect pairing dominance in several shells. The pairing gap is measured by the excitation energy of the first 2^+ state and should be independent of the neutron number. Indeed that is what the experiments tell us and what the SM-CI calculations reproduce nicely as can be seen in Fig. 1.1.

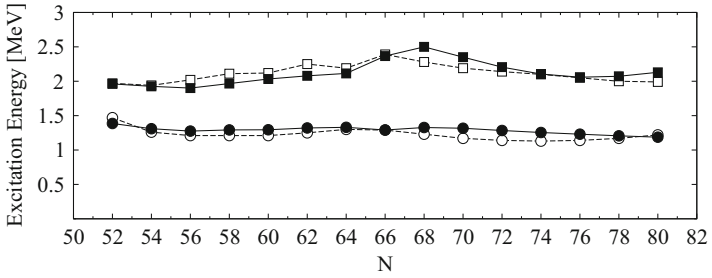

Fig. 1.1 Low energy excited states of the tin isotopes; experiment compared with SM-CI calculations in the r_4-$h_{11/2}$. space with the gcn50:82 interaction [16]; 2^+ circles, 4^+ squares, th. (filled) exp. (empty)

The problem can be turned into a dispersion relation as well. Let us write the most general solution as

$$|\alpha\rangle = \sum_j X_j^\alpha Z_j^\dagger |0\rangle \tag{1.53}$$

Plugging it in the Schrödinger equation, $H|\alpha\rangle = E_\alpha|\alpha\rangle$, we get

$$(2\epsilon_k - E_\alpha)X_k^\alpha = G\sum_j \sqrt{\Omega_j \Omega_k} X_j^\alpha \tag{1.54}$$

Multiplying by $\sqrt{\Omega_k}$ both sides and summing over k, we obtain the dispersion relation:

$$\frac{1}{G} = \sum_k \frac{\Omega_k}{2\epsilon_k - E_\alpha} \tag{1.55}$$

The dispersion relation can be solved graphically or iteratively. As we have seen before, we expect one coherent solution (the collective pair) to gain a lot of energy and the rest of the solutions to be very close to the unperturbed ones. If we assume that the single-particle energies are degenerate and take $\epsilon_k =< \epsilon >$, we obtain

$$E_\alpha = 2 < \epsilon > -G\sum_k \Omega_k \tag{1.56}$$

In this limit the energy gain is equivalent to the one in a single shell of degeneracy $\sum_k \Omega_k$.

For the case of many particles in non-degenerate orbits, the problem is usually solved in the BCS or Hartree–Fock–Bogoliubov approximations. Other approaches, which do not break the particle number conservation, are either the SM-CI or others based on it; these include the interacting boson model and its variants and different group theoretical approximations.

1.5.2 Vibrational Spectra: Quadrupole and Octupole Collectivity

In the semi-classical approach, vibrational spectra are described as the quantized harmonic modes of vibration of the surface of a liquid drop. The restoring force comes from the competition of the surface tension and the Coulomb repulsion. This is hardly germane to reality and to the microscopic description that we will develop in a simplified way. Let's just remind which are the characteristic features of a nuclear vibrator; first, a harmonic spectrum as the one shown in Fig. 1.2 and second, enhanced Eλ transitions between the states differing in one vibrational phonon.

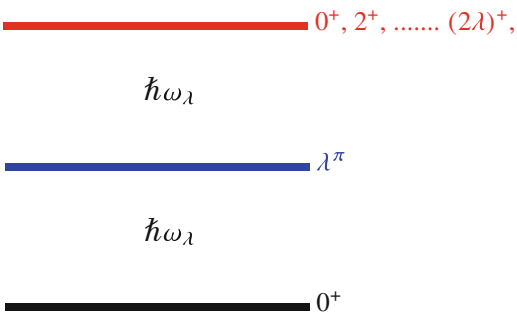

Fig. 1.2 Schematic depiction of a perfect vibrational spectrum

Imagine that for a given even-even nucleus, the orbits around the Fermi level are such as depicted in Fig. 1.3. Its ground state has $J^\pi = 0^+$, and, in the IPM, the lowest excited states correspond to promoting one particle from the occupied orbits to the empty ones. They are many, quasi-degenerate, and should appear at excitation energies Δ.

Let's take now into account the multipole Hamiltonian, which for simplicity will be of separable form, and choose as valence space just the particle-hole states, $|mi\rangle$, that correspond to making a hole in the orbit i and adding a particle in the orbit m, and then

$$\langle nj|V|mi\rangle = \beta_\lambda Q^\lambda_{nj} Q^\lambda_{mi} \tag{1.57}$$

the wave function can be developed in the p-h basis as

$$\Psi = \sum C_{mi}|mi\rangle \tag{1.58}$$

the Schödinger equation $\mathrm{H}\Psi = \mathrm{E}\Psi$ can thus be written as

$$C_{nj}(E - \epsilon_{nj}) = \sum_{mi} \beta_\lambda C_{mi} Q^\lambda_{nj} Q^\lambda_{mi} \tag{1.59}$$

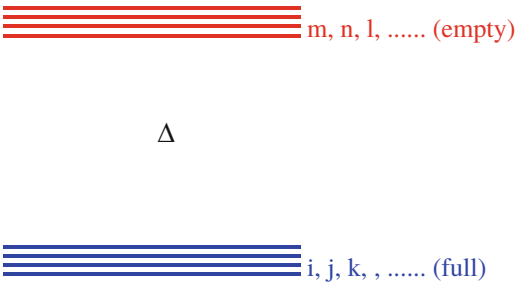

Fig. 1.3 A valence space for the description of the nuclear vibrations (see text)

and

$$C_{nj} = \frac{\beta_\lambda Q^\lambda_{nj}}{E - \epsilon_{nj}} \sum_{mi} C_{mi} Q^\lambda_{mi} \tag{1.60}$$

trivially

$$1 = \beta_\lambda \sum_{nj} \frac{(Q^\lambda_{nj})^2}{E - \epsilon_{nj}} \tag{1.61}$$

A graphical analysis of this equation shows that all its solutions except one are very close to the unperturbed values ϵ_{nj}. The remaining one is the lowest, and it is well separated from the others, very much as in the pairing case discussed before. Taking for all the ϵ_{nj} the average value $\overline{\epsilon_{nj}} = \Delta$, we obtain

$$E = \Delta + \beta_\lambda \sum_{nj} (Q^\lambda_{nj})^2 \tag{1.62}$$

If the interaction is attractive $\beta_\lambda < 0$, the lowest state gains an energy which is proportional to β_λ, the strength of the multipole interaction, and to the coherent sum of the squared one-body matrix elements of the one-body multipole operators between the particle and hole orbits in the space. This mechanism of coherence explains the appearance of vibrational states in the nucleus and represents the basic microscopic description of the nuclear "phonons". Because the couplings β_λ are constant except for a global scaling, the onset of collectivity requires the presence of several quasi-degenerate orbits above and below the Fermi level. In addition, these orbits must have large matrix elements with the multipole operator of interest.

The wave function of the coherent (collective) state (phonon, vibration) has the following form:

$$\Psi_c(J = \lambda) = \frac{\sum_{nj} Q^\lambda_{nj} |nj\rangle}{\sum_{nj} (Q^\lambda_{nj})^2} \tag{1.63}$$

The collective state is coherent with the transition operator Q^λ because the probability of its electromagnetic $E\lambda$ decay to the 0^+ ground state is very much enhanced:

$$B(E\lambda) \sim |\langle 0^+ | Q^\lambda | \Psi_c(J = \lambda)\rangle|^2 = \sum_{nj} (Q^\lambda_{nj})^2 \tag{1.64}$$

which should be much larger than the single-particle limit (many Weisskopft units (WU)). Clearly, a large value of the $B(E\lambda)$ does not imply necessarily the existence

of permanent deformation in the ground state. Notice also that nothing prevents that

$$|\beta_\lambda \sum_{nj} (Q^\lambda_{nj})^2| > \Delta \tag{1.65}$$

In this case the vibrational phonon is more bound than the ground state, and the model is no longer valid. What happens is that a phase transition from the vibrational to the rotational regime takes place as the nucleus acquires permanent deformation of multipolarity λ. The separation between filled and empty orbits does not hold anymore, and both have to be treated at the same footing.

1.6 Deformed Nuclei: Intrinsic vs. Laboratory Frame Approaches

The route to the description of permanently deformed nuclear rotors bifurcates now into laboratory frame and intrinsic descriptions. The latter include the deformed shell model (Nilsson) and the deformed Hartree–Fock approximation, plus the beyond mean field approaches such as angular momentum projection and configuration mixing with the generator coordinate method. The former, the SM-CI and in cases of full dominance of the quadrupole-quadrupole interaction group theoretical treatments like Elliott's SU(3) and its variants [17–19].

A case where the two approaches could be confronted is ^{48}Cr (four protons and four neutrons on top of ^{40}Ca) where an SM-CI description in the full *pf*-shell was for the first time possible more than two decades ago [20]. The mean field intrinsic description was a cranked Hartree–Fock–Bogoliubov (CHFB) approximation using the Gogny force. The results are presented in Fig. 1.4. Both calculations reproduce

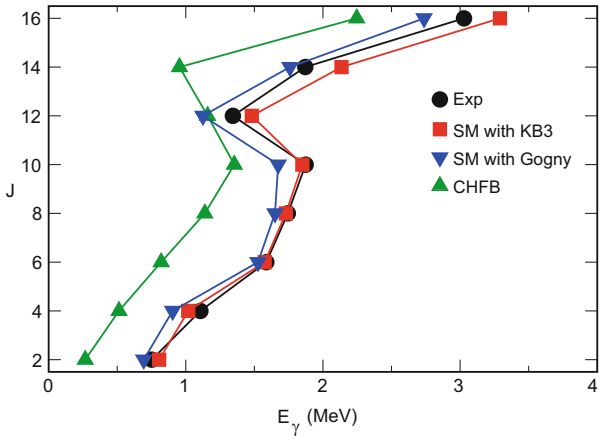

Fig. 1.4 The yrast band of ^{48}Cr; experimental data compared with the SM-CI with the KB3G interaction and the two-body matrix element of the Gogny functional and the CHFB calculations with the Gogny functional

Table 1.3 Quadrupole properties of the yrast band of ^{48}Cr, in e^2fm^4 and efm^2

J	$B(E2)_{exp}$	$B(E2)_{th}$	Q_0(t))
2	321(41)	228	107
4	330(100)	312	105
6	300(80)	311	100
8	220(60)	285	93
10	185(40)	201	77
12	170(25)	146	65
14	100(16)	115	55
16	37(6)	60	40

the rotor like behaviour at low and medium spin and the existence of a backbending at $J = 12$. However, the CHFB description misses the size of the moment of inertia due to the absence of neutron-proton pairing correlations in its wave functions. The Gogny force does contain the right proton-neutron $T = 0$ and $T = 1$ pairing as shown by the results of the SM-CI calculation with its two-body matrix elements. Hence the blame is on the CHFB method and not on the Gogny functional.

The laboratory frame wave functions are indeed collective as can be seen in Table 1.3 where we have listed the $B(E2)$s and compared with the experiment. From the calculated values, we can extract the intrinsic quadrupole moments $Q_0(t)$ using Eq. (1.85). They are roughly independent of J below the backbending as in a well-behaved Bohr–Mottelson rotor. From the intrinsic quadrupole moment, a deformation parameter can be calculated using

$$\beta = \frac{\sqrt{5\pi}}{3}\frac{Q_0(t)}{ZR^2} \tag{1.66}$$

The resulting value, $\beta = 0.28$, is in very good agreement with the CHFB result (Table 1.3).

1.6.1 The Nilsson Model

The Nilsson model is an approximation to the solution of the IPM plus a quadrupole-quadrupole interaction:

$$H = \sum_i h(\mathbf{r}_i) + \hbar\omega\kappa \sum_{i<j} Q_i \cdot Q_j \tag{1.67}$$

$$h(r) = -V_0 + \mathcal{T} + \frac{1}{2}m\omega^2 r^2 - V_{so}\mathbf{l}\cdot\mathbf{s} - V_B\mathbf{l}^2 \tag{1.68}$$

which amounts to linearizing the quadrupole-quadrupole interaction, replacing one of the operators by the expectation value of the quadrupole moment (or by the

deformation parameter). Thus, the resulting physical problem is that of the IPM subject to a quadrupole field, which obviously breaks rotational symmetry:

$$H_{Nilsson} = \sum_i h(\mathbf{r}_i) - \frac{1}{3}\hbar\omega\delta Q_0(i) \tag{1.69}$$

The problem is equivalent to the diagonalization of the quadrupole operator in the basis of the IPM eigenstates. The resulting (Nilsson) levels are characterized by their magnetic projection on the symmetry axis m, also denoted K and the parity.

The formulae below make it possible to build the relevant matrices:

$$\langle pl|r^2|pl\rangle = p + 3/2 \quad : \quad \langle pl|r^2|pl+2\rangle = -[(p-l)(p+l+3)]^{1/2} \tag{1.70}$$

$$Q_0 = 2r^2C_2 = 2r^2\sqrt{4\pi/(2l+1)}Y^{20} \quad : \quad \langle jm|C_2|jm\rangle = \frac{j(j+1)-3m^2}{2j(2j+2)} \tag{1.71}$$

$$\langle jm|C_2|j+2m\rangle = \frac{3}{2}\left\{\frac{[(j+2)^2-m^2][(j+1)^2-m^2]}{(2j+2)^2(2j+4)^2}\right\}^{1/2} \tag{1.72}$$

$$\langle jm|C_2|j+1m\rangle = -\frac{3m[(j+1)^2-m^2]^{1/2}}{j(2j+4)(2j+2)} \tag{1.73}$$

The intrinsic wave functions provided by the Nilsson model correspond to the Slater determinants built putting the neutrons and the protons in the lowest Nilsson levels (each one has degeneracy two, ±m). Therefore, for even-even nuclei $K = 0$, for odd nuclei $K = m$ of the last half occupied orbit, and for odd-odd, there are different empirical rules, not always very reliable. The Nilsson diagrams for the *sd*-shell are plotted in Fig. 1.5. The laboratory frame wave functions are obtained rotating the intrinsic frame with the Wigner matrices, i.e. correspond to the solutions of the quantum rotor problem. In the even-even case, this leads trivially to the energy formula:

$$E(J) = \sum_i (\epsilon_i)_{Nilsson} + \frac{\hbar^2}{2\mathcal{I}}J(J+1)$$

1.6.2 The SU3 Symmetry of the HO and Elliott's Model

The mechanism that produces permanent deformation and rotational spectra in nuclei is much better understood in the framework of the SU(3) symmetry of the isotropic harmonic oscillator and its implementation in Elliott's model [17]. The

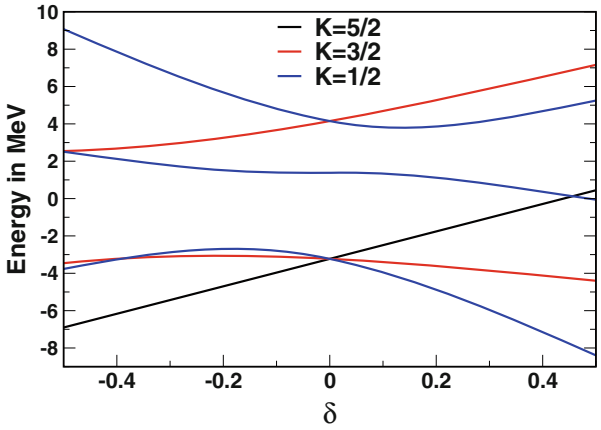

Fig. 1.5 Nilsson diagrams for the *sd*-shell: $K = 5/2$ (black), $K = 3/2$ (red) and $K = 1/2$ (blue). Energies of the states in MeV as a function of the deformation parameter

basic simplification of the model is threefold: (i) the valence space is limited to one major harmonic oscillator (HO) shell, (ii) the monopole Hamiltonian makes the orbits of this shell degenerate and (iii) the multipole Hamiltonian only contains the quadrupole-quadrupole interaction. This implies (mainly) that the spin-orbit splitting and the pairing interaction are put to zero. Let's then start with the isotropic HO which in units $m = 1\omega = 1$ can be written as

$$H_0 = \frac{1}{2}\left(p^2 + r^2\right) = \frac{1}{2}(\mathbf{p} + i\mathbf{r})(\mathbf{p} - i\mathbf{r}) + \frac{3}{2}\hbar = \hbar\left(\mathbf{A}^\dagger\mathbf{A} + \frac{3}{2}\right) \tag{1.74}$$

with

$$\mathbf{A}^\dagger = \frac{1}{\sqrt{2\hbar}}(\mathbf{p} + i\mathbf{r}) \quad \mathbf{A} = \frac{1}{\sqrt{2\hbar}}(\mathbf{p} - i\mathbf{r}) \tag{1.75}$$

which have bosonic commutation relations. H_0 is invariant under all the transformations which leave invariant the scalar product $\mathbf{A}^\dagger\mathbf{A}$. As the vectors are three-dimensional and complex, the symmetry group is U(3). We can build the generators of U(3) as bi-linear operators in the As. The antisymmetric combinations produce the three components of the orbital angular momentum L_x, L_y and L_z, which are in turn the generators of the rotation group O(3). From the six symmetric bi-linears, we can remove the trace that is a constant: the mean field energy. Taking it out we move into the group SU(3). The five remaining generators are the five components of the quadrupole operator:

$$q_\mu^{(2)} = \frac{\sqrt{6}}{2\hbar}(\mathbf{r} \wedge \mathbf{r})_\mu^{(2)} + \frac{\sqrt{6}}{2\hbar}(\mathbf{p} \wedge \mathbf{p})_\mu^{(2)} \tag{1.76}$$

The generators of SU(3) transform single-nucleon wave functions of a given p (principal quantum number) into themselves. In a single-nucleon state, there are p oscillator quanta which behave as $l = 1$ bosons. When we have several particles, we need to construct the *irreps* of SU(3) which are characterized by the Young tableaux (n_1, n_2, n_3) with $n_1 \geq n_2 \geq n_3$ and $n_1 + n_2 + n_3 = Np$(N being the number of particles in the open shell). The states of one particle in the p shell correspond to the representation $(p, 0, 0)$. Given the constancy of Np, the *irreps* can be labelled with only two numbers. Elliott's choice was $\lambda = n_1 - n_3$ and $\mu = n_2 - n_3$. In the Cartesian basis, we have $n_x = a + \mu$, $n_y = a$ and $n_z = a + \lambda + \mu$, with $3a + \lambda + 2\mu = Np$.

The quadratic Casimir operator of SU(3) is built from the generators:

$$\mathbf{L} = \sum_{i=1}^{N} \mathbf{l}(i) \qquad Q_\alpha^{(2)} = \sum_{i=1}^{N} q_\alpha^{(2)}(i) \tag{1.77}$$

as

$$C_{SU(3)} = \frac{3}{4}(\mathbf{L} \cdot \mathbf{L}) + \frac{1}{4}(Q^{(2)} \cdot Q^{(2)}) \tag{1.78}$$

and commutes with them. With the usual techniques of group theory, it can be shown that the eigenvalues of the Casimir operator in a given representation (λ, μ) are

$$C(\lambda, \mu) = \lambda^2 + \lambda\mu + \mu^2 + 3(\lambda + \mu) \tag{1.79}$$

Once these tools are ready, we come back to the physics problem as posed by Elliott's Hamiltonian:

$$H = H_0 + \chi(Q^{(2)} \cdot Q^{(2)}) \tag{1.80}$$

which can be rewritten as

$$H = H_0 + 4\chi C_{SU(3)} - 3\chi(\mathbf{L} \cdot \mathbf{L}) \tag{1.81}$$

The eigenvectors of this problem are thus characterized by the quantum numbers λ, μ and L. We can choose to label our states with these quantum numbers because O(3) is a subgroup of SU(3) and therefore the problem has an analytical solution:

$$E(\lambda, \mu, L) = N\hbar\omega(p + \frac{3}{2}) + 4\chi(\lambda^2 + \lambda\mu + \mu^2 + 3(\lambda + \mu)) - 3\chi L(L + 1) \tag{1.82}$$

This important result can be interpreted as follows: For an attractive quadrupole-quadrupole interaction, $\chi < 0$, the ground state of the problem pertains to the representation which maximizes the value of the Casimir operator, and this corresponds to maximizing λ or μ (the choice is arbitrary). If we solve the problem

in the Cartesian basis, this state is the one which has the maximum number of oscillator quanta in the z-direction, thus breaking the rotational symmetry at the intrinsic level. We can then speak of a deformed solution even if its wave function conserves the good quantum numbers of the rotation group, i.e. L and L_z. For that one (and every) (λ, μ) representation, there are different values of L which are permitted, for instance, for the representation $(\lambda, 0)$ $L = 0, 2, 4 \ldots \lambda$. And their energies satisfy the $L(L + 1)$ law, thus giving the spectrum of a rigid rotor. The problem of the description of the deformed nuclear rotors in the laboratory frame is thus formally solved.

We can describe the intrinsic states and their relationship with the physical ones using another chain of subgroups of SU(3). The chain we have used until now is SU(3)⊃O(3)⊃U(1) which corresponds to labelling the states as $\Psi([\tilde{f}](\lambda\mu)LM)$.

$[\tilde{f}]$ is the representation of U(Ω) ($\Omega = 1/2\ (p + 1)\ (p + 2)$) conjugate of the U(4) spin-isospin representation which guarantees the antisymmetry of the total wave function. For instance, in the case of ^{20}Ne, the fundamental representation (8,0) (four particles in $p = 2$) is fully symmetric, $[\tilde{f}] = [4]$, and its conjugate representation in the U(4) of Wigner [1, 1, 1, 1], fully antisymmetric. The other chain of subgroups, SU(3)⊃SU(2)⊃U(1), does not contain O(3), and therefore the total orbital angular momentum is not a good quantum number anymore. Instead we can label the wave functions as $\Phi([\tilde{f}](\lambda\mu)q_0\Lambda K)$, where q_0 is the intrinsic quadrupole moment whose maximum value is $q_0 = 2\lambda+\mu$. K is the projection of the angular momentum on the Z-axis, and Λ is an angular momentum without physical meaning. Both representations provide a complete basis; therefore it is possible to write the physical states in the basis of the intrinsic ones. Actually, the physical states can be projected out of the intrinsic states with maximum quadrupole moment as

$$\Psi([\tilde{f}](\lambda\mu)LM) = \frac{2L+1}{a(\lambda\mu KL)} \int D^L_{MK}(\omega)\Phi_\omega([\tilde{f}](\lambda\mu)(q_0)_{max}\Lambda K)d\omega \qquad (1.83)$$

Remarkably, this is the same kind of expression used in the unified model of Bohr and Mottelson, the Wigner functions D being the eigenfunctions of the rigid rotor and the intrinsic functions the solutions of the Nilsson model.

Elliott's model was initially applied to nuclei belonging to the sd-shell that show rotational features like ^{20}Ne and ^{24}Mg. The fundamental representation for ^{20}Ne is (8,0), and its intrinsic quadrupole moment, $Q_0 = (2\lambda + \mu + 3)\ b^2 = 19\ b^2 \approx 60\,\mathrm{efm}^2$ (b is the length parameter of the HO). For ^{24}Mg we have (8,4) and $23\,b^2 \approx 70\,\mathrm{efm}^2$. To compare these figures with the experimental values, we need to know

the transformation rules from intrinsic to laboratory frame quantities and vice versa. In the Bohr Mottelson model, these are

$$Q_0(s) = \frac{(J+1)\,(2J+3)}{3K^2 - J(J+1)}\, Q_{spec}(J), \quad K \neq 1 \tag{1.84}$$

$$B(E2,\, J \;\rightarrow\; J-2) = \frac{5}{16\pi}\, e^2 |\langle J\, K\, 20 | J-2,\, K\rangle|^2\, Q_0(t)^2 \quad K \neq 1/2,\, 1 \tag{1.85}$$

$$Q_{spec}(J) = < J\, J | z^2 - r^2 | J\, J > \tag{1.86}$$

The expression for the quadrupole moments is also valid in Elliott's model. However the one for the B(E2)s is only approximately valid for very low spins. Using them it can be easily verified that the SU(3) predictions compare nicely with the experimental results $Q_{spec}(2^+) = -23(3)\,\mathrm{efm}^2$ and $B(E2)(2^+ \rightarrow 0^+) = 66(3)\,\mathrm{e}^2\,\mathrm{fm}^4$ for ^{20}Ne and $Q_{spec}(2^+) = -17(1)\,\mathrm{efm}^2$ and $B(E2)(2^+ \rightarrow 0^+) = 70(3)\,\mathrm{e}^2\,\mathrm{fm}^4$ for ^{24}Mg.

Besides Elliott's SU(3) there are other approximate symmetries related to the quadrupole-quadrupole interaction which are of great interest. Pseudo-SU(3) applies when the valence space consists of a quasi-degenerate harmonic oscillator shell except for the orbit with maximum j; this space has been denoted by r_p before. Its quadrupole properties are the SU(3) ones of the shell with $(p-1)$ [18]. Quasi-SU(3) [19] applies in a regime of large spin-orbit splitting, when the valence space contains the intruder orbit and the $\Delta j = 2$, $\Delta l = 2$; $\Delta j = 4$, $\Delta l = 4$; etc., orbits which are obtained from it. Its quadrupole properties are described in Ref. [9]. These symmetries turn out to be at the root of the appearance of islands of inversion far from stability. They are more prominent at the neutron-rich side and occur when the configurations which correspond to the neutron shell closures at $N = 8$, 20, 28 and 40 are less bound than the intruder ones (more often deformed) built by promoting neutrons across the Fermi level gap. The reason of the inversion is that the intruder configurations maximize the quadrupole correlations and thus their energy gains. This is only possible when the orbits around the Fermi level can develop the symmetries of the quadrupole interaction. For instance, at $N = 20$ the intruder states in ^{32}Mg have four *sd* protons in quasi-SU(3), two *sd* neutron holes in pseudo-SU(3) and two *pf* neutrons in quasi-SU(3). This leads to a huge gain of correlation energy (typically 12 MeV) which suffices to turn the intruders into ground states.

1.7 Nuclear Deformation in the Laboratory Frame: SM-CI Approaches

As stated above, large-scale SM-CI calculations, when doable, are the spectroscopic tool of choice in theoretical nuclear structure. When they are interpreted adequately, they may provide us with the link between the experimental data and the "ab

initio" approaches. Indeed, the monopole anomaly of the realistic NN interactions may turn out to be the fingerprint of residual three-body effects [21, 22]. A non-negligible fraction of the Segré chart is nowadays amenable to SM-CI descriptions. As explained in detail in [9], the choice of a valence space which can encompass the physics dictated by the effective interaction is the crucial one in SM work. Magic numbers provide the natural borders of the SM valence spaces, because they are supposed to correspond to large gaps in the spherical mean field. Nevertheless, sometimes, if the gaps are weakened, this may not hold anymore.

The *pf*-shell provides a valence space which can cope successfully with the physics of several $N = Z$ nuclei. From the point of view of the quadrupole coupling schemes which will be dealt with in the next section, ^{48}Cr and ^{52}Fe are good quasi-SU(3)-deformed nuclei. ^{56}Ni is doubly magic albeit the closed shell amounts just to 60–70% depending on the calculations. ^{60}Zn is transitional, and ^{64}Ge looks very much like a pseudo-SU(3) mildly deformed nucleus. Beyond, we need to change the valence space [25].

The next valence space, r$_3$g, has a core of ^{56}Ni and comprises the orbits $1p_{3/2}$, $0f_{5/2}$, $1p_{1/2}$ and $0g_{9/2}$. ^{68}Se is a natural inhabitant of this space. However, its region of applicability at or close to $N = Z$ does not extend very far. Already at ^{72}Kr, oblate-prolate coexistence sets in. This requires the inclusion of the quadrupole partners of the $0g_{9/2}$ orbit, the $1d_{5/2}$ and $2s_{1/2}$ ones, in the valence space [25]. This leads to the r$_3$gds space. The next (and last) doubly magic $N = Z$ nucleus, ^{100}Sn, can be taken as the core of another valence space, r$_4$h, which spans between the magic numbers 50 and 82.

1.7.1 The Quadrupole Interaction: Intrinsic States and Coherence

In order to gauge the quadrupole coherence of a given nucleus, it is customary to compare its quadrupole properties with perfect Bohr–Mottelson rotors, i.e. to verify that the E2 transition rates and the spectroscopic quadrupole moments of the states of the yrast band can be derived from a single intrinsic quadrupole moment using Eqs. (1.84), (1.85) and (1.86).

If $Q_0(s) \approx Q_0(t)$ and constant, we can speak of good rotors. The excitation energies of the yrast band should follow approximately the $J(J+1)$ law as well. However, in light and medium mass nuclei, pairing might distort the lower part of the spectrum, giving extra binding to the 0^+ ground states. It is therefore advisable to verify the $J(J+1)$ law excluding the ground state. Another caveat here has to do with the (bad) habit of blindly extracting deformation parameters β from the $B(E2)$ values, even in cases in which the existence of an intrinsic deformed state is not guaranteed at all.

The only rigorous (but far more demanding) way of characterizing the quadrupole deformation in the laboratory frame is through the quadrupole invariants introduced by Kumar [23]. Very recently, its scope has been enlarged to make it possible to extract not only the mean values of β and γ but also their variances. Indeed, when these are very large, the notion of intrinsic state makes no sense [24].

Quadrupole coherence may be associated with a single shell (Eq. (1.71)), with a full r_p space (pseudo-SU(3)), and in this case the intrinsic single-particle states are obtained diagonalizing the quadrupole operator using Eqs. (1.71), (1.72) and (1.73) or with a full HO major shell; thus the Nilsson-like orbits of Elliott's SU3 [17] are obtained. If this is done in the $\Delta j = 2$ HO sequences (quasi SU(3)), one can diagonalize the quadrupole operator using Eqs. (1.71) and (1.72) or the corresponding expressions in *LS* coupling as adopted in [19]. We shall work with the latter choice unless explicitly stated otherwise. The radial integrals are given in Eq. (1.70). We use adimensional r^2 and $Q_0 = 2r^2C_2$ and quadrupole effective charges equal to 0.5 and 1.5 for neutrons and protons, respectively. To recover dimensions, $r^2 \rightarrow r^2b^2$.

1.7.2 The Quadrupole Interaction in a Single Orbit

The intrinsic quadrupole moment for n particles in an orbit j with principal HO quantum number p is given by the formula:

$$\frac{Q_0}{b^2} = \sum_m 2r^2\langle jm|C_2|jm\rangle = \sum_m (p+3/2)\frac{j(j+1)-3m^2}{j(j+1)} \tag{1.87}$$

If we fill orderly the magnetic sub-states with increasing $|m|$, we obtain prolate intrinsic states. If we do it the other way around, we obtain oblate intrinsic states. In Table 1.4, we list the Q_0 values for the $0g_{9/2}$ orbit and $N = Z$. For $n < (2j + 1)$ the oblate solutions have the larger Q_0 (and therefore the larger binding if the quadrupole interaction is dominant). For $n > (2j + 1)$ the prolate solutions lead. For $n = (2j + 1)$ both are degenerate.

1.7.3 SU(3) and Pseudo-SU(3)

For a full HO shell, $q_0 = 2n_z - n_x - n_y$, with $n_x + n_y + n_z = p$, where n_i are the numbers of oscillator quanta in each spatial direction. For $p = 2$, the intrinsic states are $[n_z n_x n_y] = [200], [110], [101], [020], [011], [002]$.

The quadrupole moments of the intrinsic states of the $p = 4$ shell are plotted in Fig. 1.6 (for $p = 3$ remove the upper row and change the values in the y-axis to

Table 1.4 Intrinsic quadrupole moments for n particles in the $0g_{9/2}$ orbit and $N = Z$ (in units of b^2)

n	2	4	6	8	10	12	14	16	18
Prolate	5.33	10.66	14.66	18.66	20	21.33	18.66	16	8
Oblate	−8	−16	−18.66	−21.33	−20	−18.66	−14.66	−10.66	−5.33

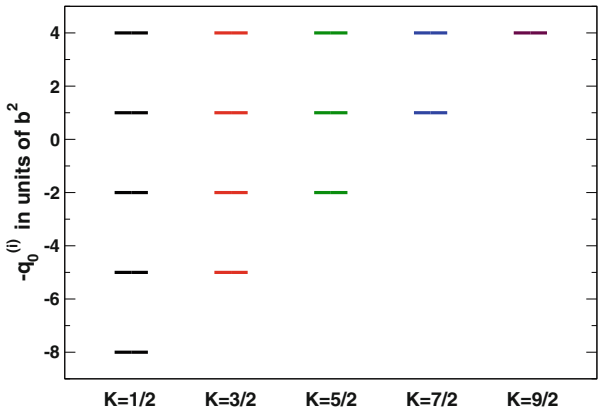

Fig. 1.6 Quadrupole moments of the intrinsic states of SU(3) for the $p = 4$ HO shell

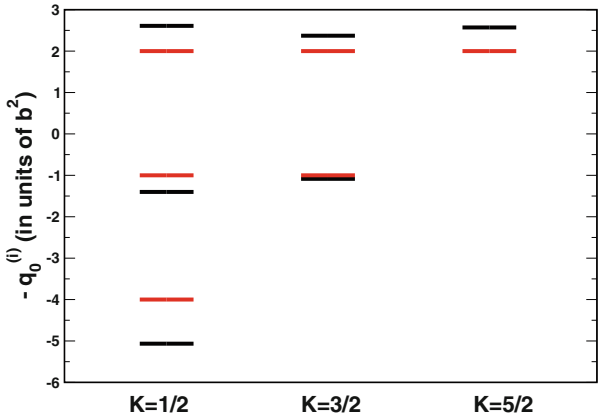

Fig. 1.7 Quadrupole moments of the intrinsic states of pseudo-SU(3) for the r_3 valence space (black) compared with those of SU(3) in the $p = 2$ HO shell (red)

$-6, -3, 0, +3$), and (for $p = 2$ remove the two upper rows and change the values in the y-axis to $-4, -1, +2$). Orderly fillings in the figure produce eigenstates of $h = qq - \lambda L(L + 1)$ and *a fortiori* rotational bands.

The values of the quadrupole moments in a pseudo-SU(3) space [18] in shell p would be the ones of SU(3) in shell p-1, except for the fact that the radial integrals are not the same. This introduces factors in the range $(p + 3/2)/(p + 1/2)$ and $\sqrt{(p + 4)/p + 2)}$. In Fig. 1.7 we have plotted the quadrupole moments in pseudo-SU(3) for the r_3 valence space compared with those of SU(3) in the $p = 2$ HO shell. Notice that the lowest prolate states have quadrupole moments that are about 20% larger than the SU(3) ones for $p = 2$.

Table 1.5 Intrinsic quadrupole moments for n holes in r_3 in the pseudo-SU(3) limit (in units of b^2)

n	2	4	6	8	10	12
Oblate	−9.74	−19.48	−22.06	−24.65	−27.20	−29.77
n	22	20	18	16	14	
Oblate	−5.14	−10.28	−15.43	−20.57	−25.17	

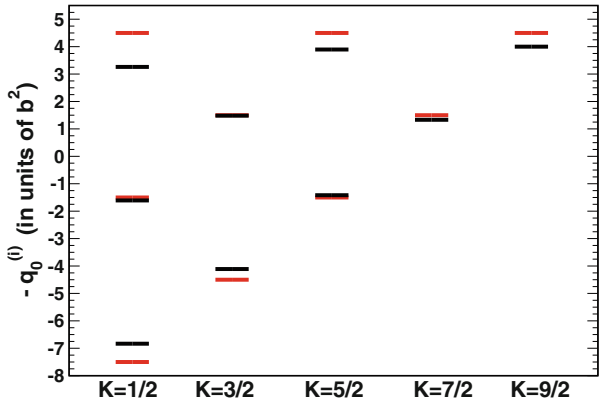

Fig. 1.8 Quadrupole moments of the intrinsic states of quasi-SU(3) for the p=4 HO shell

Table 1.6 Intrinsic quadrupole moments for n particles in the quasi-SU(3) sector of the $p = 4$ HO shell, in units of b^2, assuming $N = Z$

n	2	4	6	8	10	12	14	16
Prolate	15	30	39	48	51	54	57	60

In Table 1.5 we list the intrinsic quadrupole moments for n holes in r_3 for later use. Only the oblate solutions are explicitly included. To get the prolate ones, take for n holes the oblate value corresponding to 24-n, and change sign.

1.7.4 Quasi-SU3

In the case of a $\Delta j = 2$ HO sequence, the resulting scheme is very much like that of SU(3) except that some degeneracies are not present and the quadrupole collectivity is a bit smaller as shown in Fig. 1.8. The schematic quasi-SU(3) results are in red and the exact ones in black.

In Table 1.6 we have listed the intrinsic quadrupole moments for n particles in the quasi-SU(3) sector of the $p = 4$ HO shell. Only the prolate cases are considered. Remember that in all the SU3-like cases the total intrinsic quadrupole moment

obtained from the eigenvalues of q_0 has to be increased by 3 b^2 as explained in Ref. [26].

1.8 Coexistence: Single-Particle, Deformed and Superdeformed States in ^{40}Ca

Let's describe the structure of ^{40}Ca with a SM-CI calculation in the valence space of two major shells and interpret the results in the framework of SU(3) and its variants. The orbits of the valence space are sketched in Fig. 1.9.

The relevant configurations are $[sd]^{24}$ 0p-0h, spherical; $[sd]^{20}$ $[pf]^4$ 4p-4h, deformed (ND); and $[sd]^{16}$ $[pf]^8$ 8p-8h, superdeformed (SD).

The results presented in Fig. 1.10 show clearly the importance of the correlations. In the 8p-8h configuration, the correlations amount to 18.5 MeV. From these, 5.5 MeV is due to pairing, and the remaining 13 MeV is most likely of quadrupole

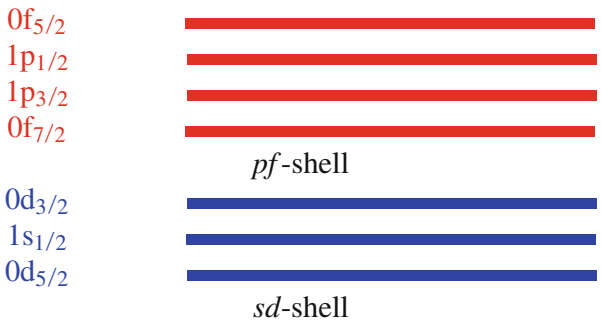

Fig. 1.9 The *sd*-*pf* valence space

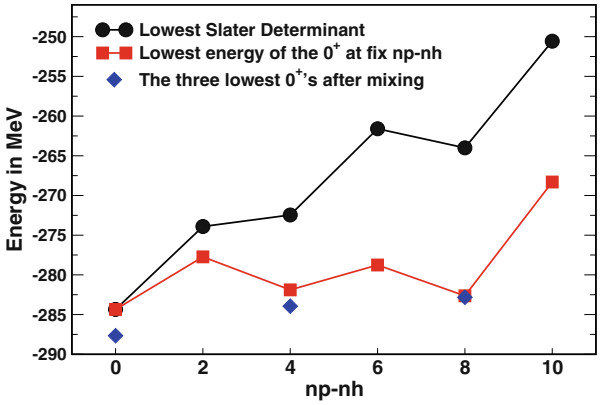

Fig. 1.10 Energies of the np-nh configurations: uncorrelated energies (blue), full mixing at fixed np-nh (black) and full mixing (red)

origin. In the 4p-4h configuration, the pairing contribution is similar, but the quadrupole one is smaller at about 4.5 MeV. The closed shell gains 5 MeV of pairing energy by mixing (30%) with the 2p-2h states, the ND band head 2 MeV and the SD band head essentially nothing.

Concerning the character of the solutions, we can see that for the 4p-4h intrinsic state of ^{40}Ca, the two neutrons and the two protons in the *pf*-shell can be placed in the lowest $K = 1/2$ quasi-SU3 level of the $p = 3$ shell. This gives a contribution to the intrinsic quadrupole moment of $q_0 = 25$ b^2. In the pseudo-*sd*-shell, $p = 2$, we are left with eight particles that contribute with $q_0 = 7$ b^2. In the 8p-8h configuration, the values are $q_0 = 35$ b^2 and $q_0 = 11$ b^2. Using the proper value of the oscillator length, it obtains:

- ^{40}Ca 4p-4h band Q_0=125 e fm^2
- ^{40}Ca 8p-8h band Q_0=180 e fm^2

These results are in very good accord with the data ($Q_0 = 120\,\text{efm}^2$ and $Q_0 = 180$ efm^2). Assuming full SU(3) symmetry in both shells, we should get $Q_0 = 148\,\text{efm}^2$ and $Q_0 = 226\,\text{efm}^2$, respectively. The SM-CI results almost saturate the quasi-SU(3) bounds. The SU(3) values are a 25% larger.

Finally we compare the SM-CI-level scheme with the experiment in Fig. 1.11. The agreement is extremely satisfactory.

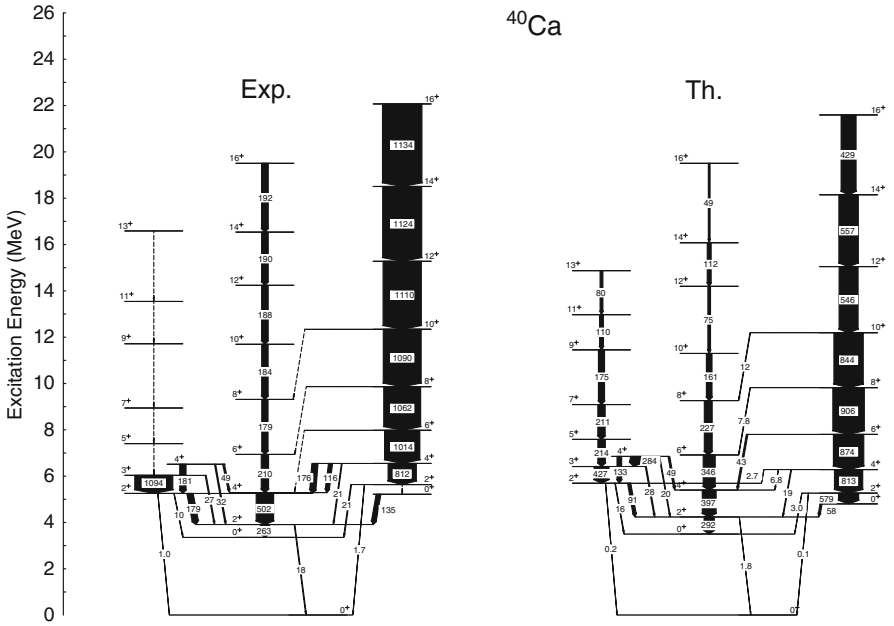

Fig. 1.11 Partial-level scheme of ^{40}Ca: Experiment (left) compared with the SM-CI results from [27] (right). The numbers in the arrows give the $B(E2)$s in e^2fm^4

1.8.1 ^{56}Ni: The Lightest Spin-Orbit Doubly Magic Nucleus

A crucial difference between the HO and the SO magic closures is that in the former the orbits below and above the Fermi level have different parities, whereas in the latter, they have the same. This implies that the lowest excited states are of positive parity and of 1p-1h nature. For instance, in ^{56}Ni the first excited state is a 2^+ at 2.7 MeV whose configuration is $(0f_{7/2})^{15}$ $(1p_{3/2})^1$. Therefore, the E2 transition to the ground state is allowed and even enhanced due to the favoured quadrupole connexion between the two orbits at play. Indeed, the experimental value amounts to 9 WU, a rather large value for a doubly magic nucleus, much larger than the corresponding one in ^{40}Ca. However, the rest of their low energy spectra resemble to each other with the appearance of low-lying 0^+ states with multiparticle-hole configuration that can be the band heads of rotational structures. This is the case of the band built on the 0^+ at 5 MeV, which, according to theory, is a 4p-4h state. As in the ^{40}Ca case, a lot of correlation energy is needed to compensate for the cost of promoting four particles across a $N = Z = 28$ gap of about 5 MeV. But we can look at it the other way round; should the gap have been slightly smaller, the deformed 4p-4h configuration would have become the ground state and ^{56}Ni expelled of the doubly magic club. In fact if one uses the original Kuo-Brown interaction, that is what occurs. In reality, due to the presence of a substantial gap, it is the quasi-degeneracy of the orbits $1p_{3/2}$, $1p_{1/2}$ and $0f_{5/2}$, which enhances the quadrupole collectivity through the action of the pseudo-SU(3) coupling and favours the polarization of the $0f_{7/2}$ orbit, as discussed in previous sections. This is another example of the relevance of the shell evolution, because these orbits, which are split apart in ^{48}Ca, become much closer in ^{56}Ni when protons fill the $0f_{7/2}$ orbit, due to the proton-neutron monopole interaction. Higher-lying bands involve excitations into the $0g_{9/2}$ orbit [28]. All in all, this is another example of the coexistence of single particle and collective degrees of freedom already at the very doubly magic nuclei.

1.9 Islands of Inversion at the Neutron-Rich Shores

Among the nuclear structure topics at the forefront of present-day experimental and theoretical research, the study of very neutron-rich nuclei plays a central role, and future facilities will make it even more prominent. We refer to three very recent review articles that give a global view of the status of the field [29–31]. A unifying theme in this research is the so-called islands of inversion (IoI). We use this term for regions of nuclei, close to a magic neutron closure, that, instead of having the expected semi-magic nature, are deformed in their ground states. The name was coined in Ref. [32] for the region surrounding ^{31}Na ($N = 20$). Reference [31] contains a detailed account of the history of the IoIs. The physics of the IoI is a prime example of the competition between the spherical mean field (a.k.a. shell evolution) and the correlations which involve excitations across the Fermi level, the same type of configurations that are responsible for the phenomenon of shape coexistence,

ubiquitous in the nuclear chart. The first IoI occurs at N=8 but was overlooked for many years, among other things, because the dominant physics there was related to the appearance of nuclear halos. We refer to [31] for the second ($N = 20$) and third ($N = 28$) ones and their merger and will dwell with the heavier ones in what follows.

1.9.1 ^{68}Ni and the $N = 40$ Island of Inversion

Twelve neutrons away from the $N = Z$ line, we reach the HO closure $N = 40$, which is the most debated one, as it only behaves like such for the protons in combination with the $N = 50$ SO closure for the neutrons in ^{90}Zr. The experimental spectrum shows a rather unclear situation: Three 0^+ states below 2.5 MeV of excitation energy, with a first excited 0^+ at 1.6 MeV and 2^+ at 2.0 MeV.

The natural valence space to capture the dynamics of this nucleus should contain at least the full pf-shell for the protons and the orbits below and above the $N = 40$ HO closure for the neutrons, i.e. $1p_{3/2}$, $1p_{1/2}$, $0f_{5/2}$, $0g_{9/2}$ and $1d_{5/2}$ (ideally the orbit $2s_{1/2}$ should be added as well). From the point of view of the development of quadrupole collectivity, this space is quite complete, because the neutron holes may live in a pseudo-SU3 regime as the proton particles do, whereas the neutron particles may take advantage of the quasi-SU(3) coupling scheme.

A monopole-adapted realistic interaction, dubbed LNPS-U, proposed for this valence space in reference [33], does provide a very satisfactory description of the level scheme of ^{68}Ni as can be seen in Fig. 1.12. According to this and other subsequent calculations, the ground state 0^+ is dominated at 65% by the doubly magic configuration $N = 40$ $Z = 28$. The second 0^+ can be said to be moderately deformed and oblate with the 2^+ and 4^+ states belonging to the same band and dominant 2p-2h (neutron) and 1p-1h (proton) configuration. The more interesting physics comes with the third 0^+ and the second 2^+ which are the germ of a highly

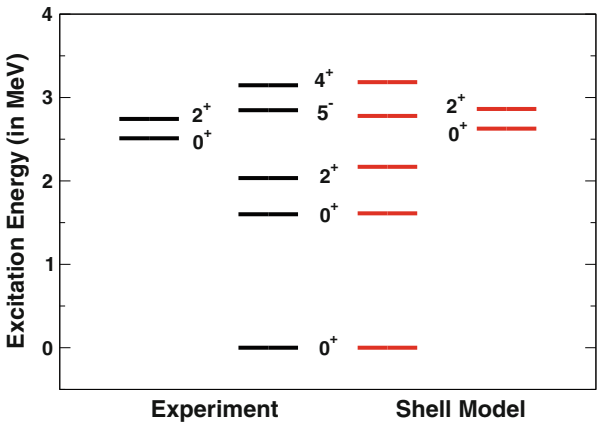

Fig. 1.12 ^{68}Ni, experiment *vs* the results of the SM-CI calculation with the interaction LNPS-U

deformed prolate band of many particle-hole structures as expected in the pseudo-plus quasi-SU(3) limit. In fact, this shape coexisting structure is the portal to the fourth IoI.

The shell evolution encoded in the LNPS-U interaction submits that at $Z = 20$, in ^{60}Ca the $N = 40$ gap is much smaller than at $Z = 28$, and the ordering of the orbits $0g_{9/2}$, $1d_{5/2}$ is inverted, a behaviour very close to that occurring in the $N = 20$ IoI between $Z = 8$, ^{28}O and doubly magic ^{34}Si. In the latter case, the orbits $0f_{7/2}$ and $1p_{3/2}$ are the ones which get inverted. It is the joint effect of the gap reduction and the quadrupole energy gains of the multiparticle-hole intruder states that produces the inversion of configurations characteristic of the IoI. The predictions of the LNPS-U calculation are displayed in Fig. 1.13 and compared with

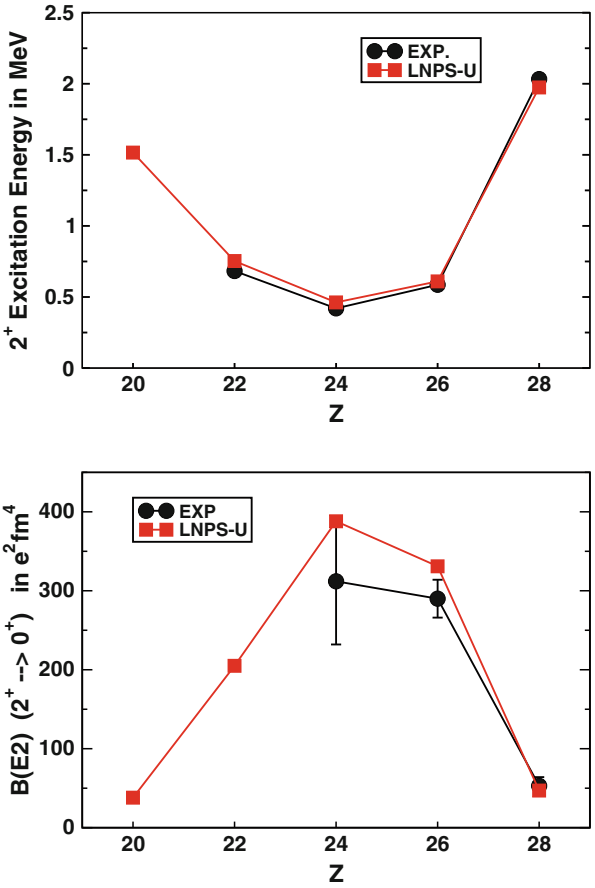

Fig. 1.13 $N = 40$ isotones, experiment *vs* the SM-CI results with the interaction LNPS-U. Excitation energy of the 2^+ (top) and $B(E2)$ (bottom)

the experimental data. The most recent measurement [34] has provided the first spectroscopic data on ^{62}Ti in full accord with the LNPS-U predictions.

Figure 1.13 shows the abrupt reduction of the excitation energy of the 2^+ and the simultaneous increase of the $B(E2)$s for ^{66}Fe, ^{64}Cr and ^{62}Ti, a signature of their location inside the IoI. As expected, their structure is very similar to that of the prolate excited band in ^{68}Ni. According to the calculations, ^{60}Ca should not be a doubly magic nucleus; instead it behaves as a pairing frustrated rotor fuelled by the neutron-neutron quadrupole interaction. A more detailed discussion can be found in ref. [31]. Therefore, neither the combination of the HO magic numbers $N = 40$, $Z = 20$ in ^{60}Ca nor $N = 40$, $Z = 40$ in ^{80}Zr survive to the competition with the quadrupole correlations.

1.9.2 ^{78}Ni: The $N = 50$ and the $N = 40$ IoI's Merge

The next milestone is ^{78}Ni, 22 neutrons away from $N = Z$. This nucleus has been a golden goal for experimentalists for decades, because it is a waiting-point nucleus candidate, whose structure, in particular whether it is doubly magic or not, has a large impact in the evolution of the r-process of nucleosynthesis. Now two HO closures are at play, $N = 50$ and $Z = 28$. From the SM-CI point of view, it has an appealing property that the valence space better suited for its description consists in two major oscillator shells, *pf* for the protons and *sdg* for the neutrons, a rather interesting circumstance. One can imagine a situation in which the $N = 50$ and $Z = 28$ gaps collapse. This would bring us close to the SU(3) limit. A back-of-an-envelope calculation using the formulas of Sect. 1.7 gives an intrinsic mass quadrupole moment $Q_0^m = 600\,\mathrm{fm}^2$ or $\beta^m = 0.45$, a huge deformation indeed, larger than the record in the region at ^{76}Sr. In reality if the gaps are large enough to preserve the doubly magic nature of ^{78}Ni, the dominant quadrupole coupling scheme is pseudo-SU(3) both for the neutrons above $N = 50$ and for the protons above $Z = 28$, whereas the holes in the $0f_{7/2}$ proton orbit and in the $0g_{9/2}$ neutron orbit add prolate coherence to the intruder configurations. Nonetheless, the maximum quadrupole coherence attainable in the realistic scheme is far from the SU(3) limit.

For the *pf*-proton *sdg*-neutron valence space, an extension of the LNPS interaction was devised, guaranteeing a smooth transition between $N = 40$ and $N = 50$. The results of this study were published in [35], and we proceed to mention its more salient aspects, keeping an eye on Fig. 1.14. First of all, the calculation supports the doubly magic character of the ground state of ^{78}Ni, with about 70% of closed $N = 50$ and $Z = 28$. The states of 1p-1h structure, depicted to the left of Fig. 1.14, are very much correlated, but without losing their identity. The lowest one is a 2^+ at about 3 MeV excitation energy. However the first excited state according to the calculation is a 0^+ that, as can be gathered visually on the right part of Fig. 1.14, is the head of a well-deformed rotational band, which is the counterpart of the one found in ^{68}Ni on top of its third 0^+, discussed in the preceding section. Here again,

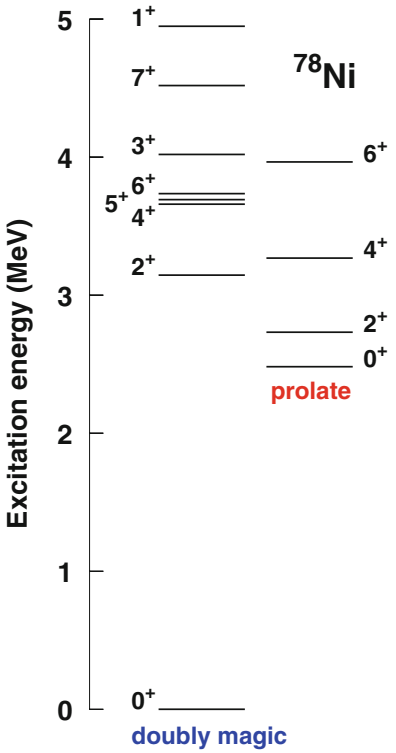

Fig. 1.14 ^{78}Ni, predictions of the SM-CI calculation with the interaction PFSDG

the coexistence of a deformed phase with the doubly magic ground state invites to surmise that another IoI might occur in the more neutron-rich isotones. It is indeed what the calculations predict, as can be seen in Fig. 1.15.

The figure shows in a very pictorial way how the deformed intruder configuration, which is excited in ^{78}Ni, becomes the ground state band as we move towards ^{70}Ca. At odds with the situation in $N = 40$, the semi-magic 0^+ state seems to survive at low excitation energy in ^{76}Fe and ^{70}Ca, causing a certain distortion of the energetics of the bands. On the contrary, the yrast band of ^{74}Cr is strictly identical to the excited band of ^{78}Ni and that of ^{72}Ti nearly so, albeit with a slightly smaller moment of inertia.

The first spectroscopy of ^{78}Ni has been obtained very recently in a groundbreaking experiment at RIKEN [36]. Two γ rays are reported which are consistent with the decays of two 2^+ states to the ground state, as predicted by the SM-CI calculations. Although the evidence is still scarce, the image of coexistence put forward by the calculation seems to be valid.

How are the fourth and fifth IoIs connected? We answer this question in Fig. 1.16. We have plotted the excitation energy of the first 2^+ as a proxy for magicity/deformation as a function of the neutron number. We compare theory and experiment where possible. The former results are obtained in the two valence

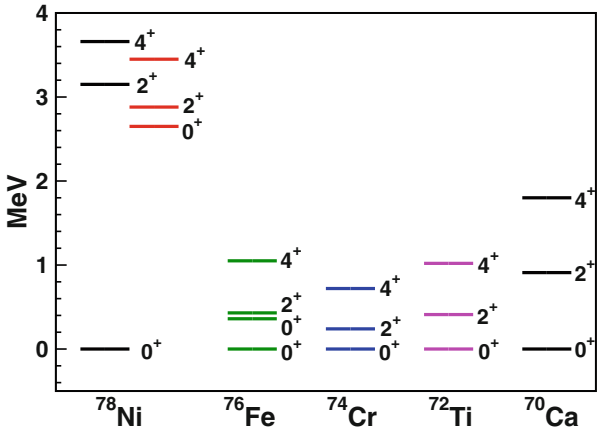

Fig. 1.15 The fifth IoI as predicted by the SM-CI calculation with the interaction PFSDG

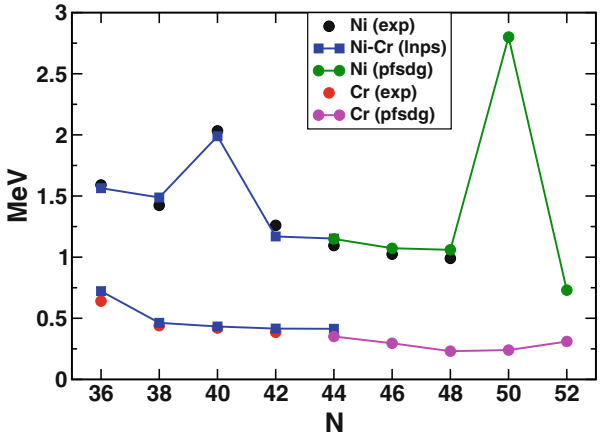

Fig. 1.16 The merging of the IoIs at $N = 40$ and $N = 50$ in the chromium isotopes, compared with the nickel chain. The excitation energy of the first 2^+ is used as control parameter

spaces discussed in this section and show clearly that the transition is smooth, with the crossover taking place around $N = 45$. Overall, the agreement with experiment is outstanding. In the nickel chain, we observe the persistence of the magic numbers $N = 40$ and $N = 50$. On the contrary, both closures are washed out in the chromium chain (in the iron and titanium as well, but we have not plotted them not to make the figure too busy), and the 2^+ excitation energy remains constant all along. Therefore we can say that the two IoIs merge. What turns out to be the same behaviour is found in the $N = 20$ and $N = 28$ IoIs for the neon, sodium and magnesium isotopes: a kind of universal behaviour indeed.

1.10 Epilogue

These lectures include a very basic introduction to the microscopic approach to the structure of the nucleus in the laboratory frame. Large-scale SM-CI calculations are a safe way to approach the exact solution of the many-body problem. However the explosion of the dimensions of the basis to be used prevents the brute force treatment. Hence, one must resort to the use of effective theories to design valence spaces that contain the more relevant degrees of freedom, renormalizing consistently the Hamiltonian and the transition operators. But, another ingredient, particular to the nuclear system, is the uncertainty of our knowledge of the nucleon-nucleon interaction, and it's poorly known many-body terms. As we have discussed in detail, close-to-exact solutions of the nuclear many-body problem for few nucleon systems (VMC, NCSM) require the explicit use of three-body forces in order to explain the full body of experimental data. Nuclear interactions obtained in χ-EFT do produce such three-body interactions naturally.

Our endeavour, monopole-adapted interaction, plus multipole-guided valence spaces, offers a solid bridge between the purely phenomenological approach, based on the fit of all the two-body matrix elements in a given valence space to the available experimental data (pioneered by B. H. Wildenthal and his USD interaction [37]), and the "ab initio" campaign (see, for instance, [4]).

We submit, and we have explained it in these lectures that once the monopole behaviour is corrected, the pairing and the multipole-multipole contents of the realistic interactions obtained via renormalized G-matrices make it possible to reproduce a large amount of experimental data with great accuracy and in some cases to predict new physics, as, for instance, the existence of IoIs. It is important to recall that the monopole Hamiltonian is responsible for all the extensive properties of the nucleus, basically its saturation point in the Coester plot, one of the long-standing problems in nuclear physics which appears in the nuclear spectroscopy hidden in the shell evolution. No reason for the latter to be right if the former is wrong. In a nutshell, we rely in these three pillars: the multipole part of the realistic interactions, a monopole Hamiltonian which reproduces what is experimentally known of the spherical mean field evolution with N and Z and the invaluable help of the SU(3) heuristic to define the minimal valence spaces to be used in the SM-CI approach.

How to make explicit the connection with the "ab initio" program? Indeed we all will be more than happy if there were a single QCD complying NN+NNN+? interaction and a rigorous reduction of these bare interactions to tractable Fock space bases. This is not the case yet, because the number of χ-EFT interactions is still too large, and sometimes the better ones for the many-body problem are not the best for the two- and three-body cases (see the contribution of R. Roth in this volume for a detailed description of the present state of the field). At present, the final step of the "ab initio" approach, from a spectroscopic point of view, consists in the derivation of two-body interactions to be used in SM-CI diagonalizations (VS-IMSRG). Hence, they are subject to the same dimensionality limitations of the

standard SM-CI calculations. Obviously, they also rely in a physically sound choice of the valence spaces. We are afraid that the sensitivity of the outcome of the SM-CI calculations to (not so big) modifications of the spherical mean field can make it difficult for the "pure ab initio" approach to reach an optimum level of spectroscopic quality. However, the mere fact of understanding the monopole crisis of the realistic interactions in terms of three-body forces is a huge step ahead in our mastering on the nuclear dynamics. Another important asset of the "ab initio" calculations are the studies of the basic physics involved in the quenching of the $\sigma\tau$ (and related) operators in the nucleus, most notably in the neutrinoless double beta decay process. But, in our opinion, a first meeting point, and a much simpler one, would be to produce a kind of "ab initio" monopole Hamiltonian including three-body terms.

Finally, let us mention that in order to overcome the dimensionality barriers of the SM-CI calculations, there is a new line of thought that proposes the use of beyond mean field techniques, like projected Hartree–Fock plus generator coordinator configuration mixing, in shell model valence spaces, which we find very promising [38, 39].

Disclaimer In these lectures we have drawn freely from many standard nuclear structure books. In particular:

- P. Ring and P. Schuck, The Nuclear Many-Body Problem (Springer 1980)
- K. Heyde, The Nuclear Shell Model (Springer 1994)
- A. Bohr and B. Mottelson, Nuclear Structure, vols. I y II, (World Scientific 1998)
- J. Suhonen, From Nucleons to Nucleus (Springer 2007)
- A. De Shalit and H. Feshbach, Theoretical Nuclear Physics, vol I, Nuclear Structure (Wiley 1974)
- P. Brussaard and P. Glaudemans, Shell Model Applications in Nuclear Spectroscopy (North Holland 1977)
- I. Talmi, Simple Models of Complex Nuclei (Harwood, 1993)
- G. Brown, Unified Theory of Nuclear Models and Forces (North Holland 1971)

For the less standard aspects of the presentation, we follow the work of the Strasbourg Madrid Shell Model collaboration, notably the review of Ref. [9].

Acknowledgments AP's work is supported in part by the Ministerio de Ciencia, Innovación y Universidades (Spain), Grant CEX2020-001007-S funded by MCIN/AEI/10.13039/501100011033 and Grant PGC-2018-94583.

References

1. S.C. Pieper, V.R. Pandharipande, R.B. Wiringa, J. Carlson, Phys. Rev. C **64**, 011401 (2001)
2. P. Navratil, W.E. Ormand, J.P. Vary, B.R. Barret, Phys. Rev. Lett. **87**,172501 (2001)
3. E. Epelbaum, H. Krebs, D. Lee, Ulf-G. Meissner, Phys. Rev. Lett. **106**, 192501 (2011)
4. S.R. Stroberg, H. Hergert, S.K. Bogner, J.D. Holt, Ann. Rev. Nucl. Part. Sci. **69**, 307 (2019)

5. V.R. Pandharipande, I. Sick, P.K.A, deWitt Huberts, Rev. Mod. Phys. **69**, 981 (1997)
6. D.M. Brink, E. Boeker, Nucl. Phys. A **91**, 1 (1967)
7. J. Dechargé, D. Gogny, Phys. Rev. C **21**, 1569 (1980)
8. J.M. Cavedon et al., Phys. Rev. Lett. **49**, 978 (1982)
9. E. Caurier, G. Martínez-Pinedo, F. Nowacki, A. Poves, A.P. Zuker, Rev. Mod. Phys. **77**, 427 (2005)
10. T.A. Brody, M. Moshinsky, *Tables of Transformation Brackets for Nuclear Shell-Model Calculations* (Gordon and Breach Science Publishers, New York, 1967)
11. K. Heyde, *The Nuclear Shell Model* (Springer, Berlin,1994)
12. M. Dufour, A.P. Zuker, Phys. Rev. C **54**, 1641 (1996)
13. B. A. Brown et al., OXBASH code, MSU-NSCL technical report 524 (1985)
14. B.A. Brown, W.D.M. Rae, Nucl. Data Sheets **120**, 115 (2014)
15. N. Shimizu, T. Mizusaki, Y. Utsuno, Y. Tsunoda, Comput. Phys. Commun. **244**, 372 (2019)
16. E, Caurier, F. Nowacki, A. Poves, K. Sieja, Phys. Rev. C **82**, 064304 (2010)
17. J.P. Elliott, Proc. R. Soc. Lond. Ser. A **245**, 128 (1956)
18. A. Arima, M. Harvey, K. Shimizu, Phys. Lett. B **30**, 517 (1969); K. Hecht, A. Adler, Nucl. Phys. A **137**, 129 (1969)
19. A.P. Zuker, J. Retamosa, A. Poves, E. Caurier, Phys. Rev. C **52**, R1741 (1995)
20. E. Caurier, J.L. Egido, G. Martínez-Pinedo, A. Poves, J. Retamosa, L.M. Robledo, A.P. Zuker, Phys. Rev. Lett. **75**, 2466 (1995)
21. A.P. Zuker, Phys. Rev. Lett. **90**, 042502 (2003)
22. P. Navratil, W.E. Ormand, Phys. Rev. Lett. **88**, 152502 (2002)
23. K. Kumar, Phys. Rev. Lett. **28**, 249 (1972)
24. A. Poves, F. Nowacki, Y. Alhassid, Phys. Rev. C **101**, 054307 (2020)
25. A.P. Zuker, A. Poves, F. Nowacki, S.M. Lenzi, Phys. Rev. C **92** 024320 (2015)
26. J. Retamosa, J.M. Udias, A. Poves, E. Moya de Guerra, Nucl. Phys. A **511**, 211 (1990)
27. E. Caurier, J. Menéndez, F. Nowacki, A. Poves, Phys. Rev. C **75** 054317 (2007)
28. D. Rudolf et al., Phys. Rev. Lett. **82**, 3763 (1999)
29. O. Sorlin, M.-G. Porquet, Prog. Part. Nucl. Phys. **61**, 602 (2008)
30. T. Otsuka, A. Gade, O. Sorlin, T. Suzuki, Y. Utsuno, Rev. Mod. Phys. **92**, 015002 (2020)
31. F. Nowacki, A. Poves, A. Obertelli, Prog. Part. Nucl. Phys. **120** 103866 (2021)
32. E.K. Warburton, J.A. Becker, B.A. Brown, Phys. Rev. C **41**, 1147 (1990)
33. S.M. Lenzi, F. Nowacki, A. Poves, K. Sieja, Phys. Rev. C **82**, 054301 (2010)
34. M. L. Cortes et al., Phys. Lett. B **800**, 135071 (2020)
35. F. Nowacki, A. Poves, E. Caurier, B. Bounthong, Phys. Rev. Lett. **117**, 272501 (2016)
36. R. Taniuchi et al., Nature **569**, 53 (2019)
37. B.H. Wildenthal, Prog. Part. Nucl. Phys. **11**, 5 (1984)
38. A. Sánchez-Fernández, B. Bally, T.R. Rodríguez, Phys. Rev. C **104**, 054306 (2021)
39. D. Duy Duc, F. Nowacki, Phys. Rev. C **105**, 054314 (2022)